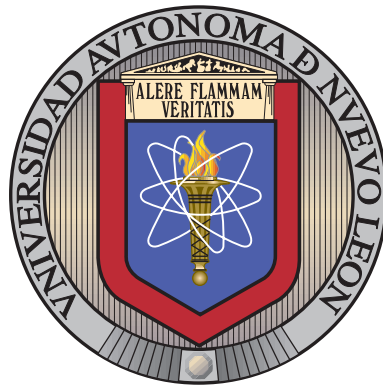


UNIVERSIDAD AUTÓNOMA DE NUEVO LEÓN

FACULTAD DE INGENIERÍA MECÁNICA Y ELÉCTRICA

SUBDIRECCIÓN DE ESTUDIOS DE POSGRADO



OPTIMIZACIÓN E INFERENCIA EN PROCESOS FÍSICO-QUÍMICOS  
REPRESENTADOS MEDIANTE AUTÓMATAS CELULARES

POR

M. C. LUIS ALEJANDRO BENAVIDES VÁZQUEZ

COMO REQUISITO PARCIAL PARA OBTENER EL GRADO DE

DOCTORADO EN INGENIERÍA

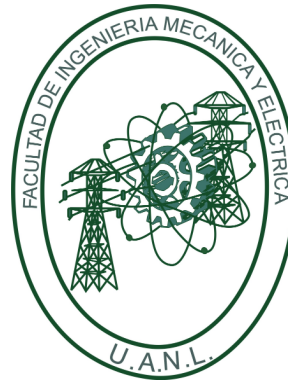
CON ESPECIALIDAD EN INGENIERÍA DE SISTEMAS

DICIEMBRE 2017

UNIVERSIDAD AUTÓNOMA DE NUEVO LEÓN

FACULTAD DE INGENIERÍA MECÁNICA Y ELÉCTRICA

SUBDIRECCIÓN DE ESTUDIOS DE POSGRADO



OPTIMIZACIÓN E INFERENCIA EN PROCESOS FÍSICO-QUÍMICOS  
REPRESENTADOS MEDIANTE AUTÓMATAS CELULARES

POR

M. C. LUIS ALEJANDRO BENAVIDES VÁZQUEZ

COMO REQUISITO PARCIAL PARA OBTENER EL GRADO DE

DOCTORADO EN INGENIERÍA

CON ESPECIALIDAD EN INGENIERÍA DE SISTEMAS

DICIEMBRE 2017

# Universidad Autónoma de Nuevo León

## Facultad de Ingeniería Mecánica y Eléctrica

### Subdirección de Estudios de Posgrado

Los miembros del Comité de Tesis recomendamos que la Tesis “OPTIMIZACIÓN E INFERENCIA EN PROCESOS FÍSICO-QUÍMICOS REPRESENTADOS MEDIANTE AUTÓMATAS CELULARES”, realizada por el alumno M. C. Luis Alejandro Benavides Vázquez, con número de matrícula 1373078, sea aceptada para su defensa como requisito parcial para obtener el grado de Doctorado en Ingeniería con Especialidad en Ingeniería de Sistemas.

El Comité de Tesis

---

Dr. José Arturo Berrones Santos

Asesor

---

Dra. Satu Elisa Schaeffer

Co-asesora

---

Dr. Francisco Javier Almaguer Martínez

Revisor

---

Dr. César Emilio Villarreal Rodríguez

Revisor

---

Dra. Mónica María Alcalá Rodríguez

Revisora

Vo. Bo.

---

Dr. Simón Martínez Martínez

Subdirector de Estudios de Posgrado

San Nicolás de los Garza, Nuevo León, diciembre 2017

*A mis padres*  
*Bertha Alicia y*  
*José Loreto*

*A mi hermano*  
*José Alberto*

*A mi prometida*  
*Margarita Cadena*

# AGRADECIMIENTOS

---

Deseo agradecer a la Universidad Autónoma de Nuevo León (UANL) la oportunidad que me brindó para realizar mis estudios de posgrado.

A la Facultad de Ingeniería Mecánica y Eléctrica (FIME) por el apoyo brindado durante mis estudios de doctorado.

Al Consejo Nacional de Ciencia y Tecnología (CONACYT) por el apoyo económico otorgado mediante una beca de estudios de tiempo completo.

Quedo agradecido al Posgrado de Maestría en Ingeniería de Sistemas (PISIS) por darme la oportunidad de realizar mis estudios de doctorado.

Quiero expresar mi agradecimiento al Dr. Arturo Berrones Santos, director de la tesis, por haberme guiado durante todo este tiempo, darme consejos para mejorar en mis habilidades de análisis y escritura los cuales me han ayudado a mejorar tanto profesional como personalmente. Además de brindarme su apoyo y su amistad.

De la misma manera, agradezco a la Dra. Elisa Schaeffer, co-asesora de la tesis, quien me brindó su apoyo y enseñanza durante el trayecto del doctorado. Me ayudó a mejorar sustancialmente las deficiencias con las que llegué al doctorado. Gracias por todo y espero seguir realizando colaboraciones con usted.

Agradezco al Dr. Javier Almaguer por ser parte de mi comité de tesis, guiarme

---

como ayuda en la elaboración de la misma. Además, de mejorar mis habilidades de análisis teórico de los temas presentados en la tesis y brindarme su apoyo con los conceptos que más se me dificultaron durante la tesis.

Agradezco a la Dra. Mónica Alcalá por guiarme en la parte experimental de la tesis y ser parte de mi comité de tesis.

Agradezco al Dr. César Villarreal por ser parte de mi comité de tesis y guiarme como ayuda en la elaboración de la misma.

Deseo agradecer a todos los profesores y compañeros del PISIS por su compañía y ayuda durante mi estancia en el doctorado.

Agradezco profundamente a mi familia: mis padres Bertha Alicia y José Loreto, así como a mi hermano José Alberto, que siempre estuvieron para apoyarme en el transcurso de mis estudios de doctorado tanto en el ámbito personal y profesional, con sus consejos, siempre motivándome para enfrentar las adversidades que se presenten y esforzándose para sacar lo mejor de mí con el fin de mejorarme en cada situación que se me presenta. Gracias a ustedes he podido completar esta meta y podré completar cualquier cosa que me proponga.

Agradezco de todo corazón a mi prometida Margarita Cadena por comprenderme y apoyarme incondicionalmente durante el trayecto del doctorado. Además, por estar siempre a mi lado, hacer de mí una mejor persona con ayuda de tus consejos para conseguir todo lo que me proponga. Todo esto me ha ayudado a terminar esta etapa. Juntos seguiremos mejorando tanto personal y profesionalmente, cumpliendo cualquier reto que se nos presente.

# RESUMEN

---

M. C. Luis Alejandro Benavides Vázquez.

Candidato para obtener el grado de Doctorado en Ingeniería con Especialidad en Ingeniería de Sistemas.

Universidad Autónoma de Nuevo León.

Facultad de Ingeniería Mecánica y Eléctrica.

Título del estudio: OPTIMIZACIÓN E INFERENCIA EN PROCESOS FÍSICO-QUÍMICOS REPRESENTADOS MEDIANTE AUTÓMATAS CELULARES.

Número de páginas: 99.

**OBJETIVOS Y MÉTODO DE ESTUDIO:** Un autómata celular probabilístico Markoviano para capturar el fenómeno esencial de la ruptura y agregación en presencia de agitación externa es propuesto y su espacio de parámetros es explorado a fondo. El modelo propuesto es una extensión multidimensional de un modelo conceptual unidimensional, el cual logró reproducir algunas características básicas de la distribución del tamaño de partículas en la remoción de metales pesados en una prueba de jarras. Reportamos experimentos numéricos del espacio de parámetros para el autómata multidimensional para identificar los parámetros que mejor reproducen la distribución de tamaño de partículas observada, obteniéndose un mejor acuerdo

---

cuantitativo que el modelo original y reproduciendo de manera robusta las características del sistema real.

CONTRIBUCIONES Y CONCLUSIONES: El modelo de autómata multidimensional presentado mejora el ajuste cuantitativo de las distribuciones de tamaño de flóculo observadas en laboratorio: capta las distribuciones de tamaño de partículas para los datos de laboratorio de remoción de aguas residuales de metales pesados con precisión más alta que nuestra experimentación con el modelo unidimensional basado en el modelo anterior. Por lo que nuestro modelo provee una alternativa intuitiva y computacionalmente eficiente a los modelos integro-diferenciales con ecuaciones acopladas.

Firmas de los asesores: \_\_\_\_\_

Dr. José Arturo Berrones Santos

\_\_\_\_\_  
Dra. Satu Elisa Schaeffer

# ABSTRACT

---

Luis Alejandro Benavides Vázquez, M. Sc.

Candidate for obtaining the degree of Doctorate in Engineering with Specialization in Systems Engineering.

Universidad Autónoma de Nuevo León.

Facultad de Ingeniería Mecánica y Eléctrica.

Title of the study: OPTIMIZATION AND INFERENCE IN PHYSICAL-CHEMICAL PROCESSES REPRESENTED BY A CELLULAR AUTOMATON.

Number of pages: 99.

**OBJECTIVES AND METHODS:** A Markovian probabilistic cellular automaton to capture the essential phenomenology of coalescence and fragmentation in the presence of external agitation is proposed and its parameter space is thoroughly explored. The proposed model is a multi-dimensional extension of a one-dimensional conceptual model, reported to reproduce some basic features of floc-size distribution of heavy-metal wastewater removal in a jar-test apparatus. We report extensive numerical experiments of the parameter spaces for multi-dimensional automaton to identify those that best reproduce observed floc-size distributions; the proposed extension yields better quantitative agreement than the original model and reproduces in a

---

more robust manner characteristic features of the real-world system.

CONTRIBUTIONS AND CONCLUSIONS: The presented multi-dimensional model improves the quantitative agreement with the laboratory-observed floc-size distributions: it captures floc-size distributions for laboratory data from a heavy-metal wastewater removal experiment with higher accuracy than our experimentation with the previous one-dimensional model. The proposed multi-dimensional model therefore provides an alternative that is computationally more efficient as well as more intuitive than integro-differential coupled equation models.

Signatures of supervisors: \_\_\_\_\_  
Dr. José Arturo Berrones Santos

\_\_\_\_\_  
Dra. Satu Elisa Schaeffer

# CONTENTS

---

<b>Agradecimientos</b>	<b>v</b>
<b>Resumen</b>	<b>vii</b>
<b>Abstract</b>	<b>ix</b>
<b>1 Introduction</b>	<b>1</b>
1.1 Hypothesis . . . . .	4
1.2 Objective . . . . .	4
1.3 Structure of the Thesis . . . . .	4
<b>2 Background</b>	<b>6</b>
2.1 Wastewater Treatment . . . . .	6
2.1.1 Coalescence-Fragmentation Process . . . . .	8
2.1.2 Jar-Test Apparatus . . . . .	11
2.2 Mathematical Models . . . . .	13

---

2.2.1	Differential Equations . . . . .	14
2.2.2	Stochastic Processes . . . . .	15
2.2.3	Cellular Automaton Theory . . . . .	17
2.2.4	Urn Model . . . . .	20
<b>3</b>	<b>Literature Review</b>	<b>22</b>
3.1	Coalescence-Fragmentation Process . . . . .	22
3.2	Coalescence Process . . . . .	25
3.3	Population Balance Equation . . . . .	27
3.4	Floc Distribution . . . . .	30
3.5	Wastewater Treatment Applications . . . . .	31
3.6	Laboratory Analysis . . . . .	32
3.7	Cellular Automaton . . . . .	33
3.8	Other Similar Processes . . . . .	36
3.9	Discussion . . . . .	37
<b>4</b>	<b>Methodology</b>	<b>39</b>
4.1	Case Study: Wastewater Removal . . . . .	40
4.2	Probabilistic Models . . . . .	44
4.2.1	Multi-Dimensional Cellular-Automaton Model . . . . .	45

---

4.2.2	Urn Model . . . . .	49
4.3	Differential Equation Model . . . . .	51
4.3.1	Constant Coalescence Rate . . . . .	53
4.3.2	Additive and Multiplicative Coalescence Rates . . . . .	56
<b>5</b>	<b>Computational Experiments</b>	<b>58</b>
5.1	Implementation of the Cellular Automaton Model . . . . .	59
5.2	Experimental Setup . . . . .	60
5.2.1	Validation . . . . .	62
5.2.2	Comparison with Previous Model . . . . .	68
5.2.3	Parameter-Space Exploration . . . . .	69
<b>6</b>	<b>Conclusions</b>	<b>80</b>
6.1	Contributions . . . . .	81
6.2	Discussion . . . . .	81
6.3	Future Work . . . . .	82
	<b>Bibliography</b>	<b>84</b>

# LIST OF FIGURES

---

2.1	Typical setup of a jar-test apparatus. . . . .	11
2.2	The principal steps of the jar test. . . . .	12
2.3	Von Neumann neighborhood for a one-dimensional automaton. . . . .	18
2.4	Von Neumann neighborhood for a two-dimensional automaton. . . . .	18
2.5	An example of a two-dimensional regular Cellular Automaton. . . . .	19
2.6	An example of a two-dimensional borderless Cellular Automaton. . . . .	19
4.1	Microscopic images of the flocculation process, for the data set 1, observed at five different agitation times for iron chloride at an agitation speed of 20 rpm. . . . .	42
4.2	Microscopic images of the flocculation process, for the data set 2, observed at five different agitation times for iron chloride at an agitation speed of 25 rpm. . . . .	43
4.3	Experimental floc-size distribution for iron chloride at an agitation speed of 40 rpm after seven minutes of agitation. . . . .	44
4.4	A visualization of a stationary state of a two-dimensional automaton. . . . .	46

---

4.5	Example of a sigmoid function. . . . .	51
4.6	Example of an exponential distribution. . . . .	51
5.1	Visual representation of the mass flux of $J_k$ to $J_{k+1}$ . . . . .	63
5.2	Comparison between four dimensions reaching a gel state as a function of the steps. . . . .	64
5.3	Average Manhattan distances between cells as a function of the di- mension of the automaton. . . . .	65
5.4	Linear growth of the floc-size distribution mean of the automaton relative to $\bar{h}$ . . . . .	67
5.5	Second-order polynomial growth of the floc-size distribution variance relative to $\bar{h}$ . . . . .	67
5.6	A stationary state with large mean and variance of the floc-size dis- tribution relative to $\bar{h} = 3$ is reported for $f = 0.9$ and $v = 0.1$ . . . . .	68
5.7	Comparison of the floc-size distribution between our one-dimensional cellular automaton, the previous one-dimensional cellular automaton from by Almaguer et al. [4], and the laboratory data. . . . .	70
5.8	The four laboratory-experiment steady states in terms of the propor- tion of large flocs. . . . .	72
5.9	The proportion of large flocs evolution an example simulation accord- ing to the step count where a steady state and two outliers exist. . . . .	73
5.10	Examples with and without an overlap between the laboratory exper- iment and the simulation intervals. . . . .	76

# LIST OF TABLES

---

5.1	Parameters of the simulation for the one-dimensional cellular automaton as reported by Almaguer et al. [4]. . . . .	69
5.2	Normality results for the Shapiro-Wilks test in each laboratory-experiment data using the large flocs variation. . . . .	71
5.3	Normality results for the Shapiro-Wilks test in a sample of the simulation data using proportion of large flocs data without outliers. . . .	74
5.4	Top five parameter combinations $f$ , $v$ , and $d$ of the automaton compared with each laboratory experiment using a similarity threshold greater or equal to 0.59. . . . .	79

## CHAPTER 1

# INTRODUCTION

---

In Mexico, water treatment is an issue that involves national security and has become central to the environmental and economic policies, as well as a key factor of social development. It is important that wastewater discharges do not mix to ensure that clean water is provided to meet the needs of the population and contribute to economic growth and quality of life [34].

The removal of heavy metals in wastewater is expensive. The industry must dedicate significant budgets for fees that include contamination, bad treatment, and *floc* (that is, a group of particles joined together to form a larger entity) size of contaminants, among others. An important problem in Mexican industries is the selection and dosage of chemical coagulants into the wastewater to promote floc formation for its removal. Other questions of interest are determining the speed at which the largest flocs are formed and the moment at which to carry out the filtration. Usually, the decisions for these issues are made based on the operator's previous experience with jar-test apparatus experiments [99].

Our motivation for the present work is *wastewater treatment*: coalescence-promoting chemicals are mixed with wastewater to achieve *flocculation*, i.e., the

formation of flocs in the suspended solids with sufficient size for the flocs to settle or be removed [2, 95]. External *agitation* may improve the floc formation but also promote instabilities that may fracture the flocs. Hence, our interest focuses towards kernels that are influenced by an agitation speed, the primary goal being the identification of experimental conditions for which the resulting floc-size distribution has an ideal shape for their removal from the wastewater.

One of the most studied mechanisms are coalescence-fragmentation processes due to their presence on application such as colloidal chemistry, polymer science, magnetic nanoparticles suspensions, and wastewater treatment, among many others [40, 63, 102, 115, 119]. The usual approach is the framework given by the coalescence-fragmentation equation [42, 115]:

$$\frac{d\rho_n}{dt} = \frac{1}{2} \sum_{i+j=n} [\rho_i \rho_j A_{i,j} - \rho_{i+j} F_{i,j}] - \sum_{j=1}^{\infty} [\rho_k \rho_j A_{n,j} - \rho_{n+j} F_{n,j}]. \quad (1.1)$$

Equation (1.1) is a particular case of the *Smoluchowski balance equation*: a mean-field description that provides no information regarding spatial dependencies or fluctuations. Equation (1.1) describes the evolution of the density of a *floc*  $\rho_n$  (a cluster of  $n$  aggregated particles, where  $n$  is the size of a floc) according to the densities  $\rho_i$ . The coalescence kernel  $A_{ij}$  is the reaction rate for an aggregation of a size  $i$  floc with a size  $j$  floc, and the fragmentation kernel  $F_{ij}$  is the reaction rate for a fragmentation of a size  $i + j$  into one floc of size  $i$  and another floc of size  $j$ . The multiplier  $\frac{1}{2}$  is included to eliminate the effect of having counted twice the interactions of floc sizes  $i$  and  $j$  (for example,  $1 + 2 = 3$  and  $2 + 1 = 3$  for  $n = 3$ ). The term coalescence is also known as *aggregation* (two or more flocs are aggregated to form one single floc), whereas fragmentation is sometimes called *break-up* (a floc breaks into two or more) in the literature.

The mathematical solution of Equation (1.1) is an active research area [10, 11]

where the analysis is centered in the study of the particular solutions by simplifications in the kernel rates. A simplification occurs only when pure coalescence is present ( $F = 0$ ), leading to stationary solutions of Equation (1.1) that give rise to a single floc in infinite times with statistical properties that depend on the coalescence kernel  $A$ . When  $F > 0$ , stationary states may emerge. If only fragmentation exists ( $A = 0$ ), the flocs at infinite times tend to stay at a certain size depending on the initial condition. If both mechanisms are included, the tractability of the Equation (1.1) grows due to all interactions, so it is necessary to develop a simulation technique that captures the expected behavior of the coalescence-fragmentation while simultaneously simplifying the calculations involved in the interactions between flocs.

A popular model to simulate interactions between flocs is the *cellular automaton*. This model has been employed for different applications in nature and specially in chemistry process [25, 73, 111]. We focus on one application that captures the essential phenomenon of coalescence-fragmentation processes in the presence of external agitation [4]. One of the principal problems in these processes is to determine the interaction rule between the cells. Another problem is to determine the range of the parameters that promote the ideal floc sizes for their removal.

In the first years of study of cellular automaton, different statistical and probabilistic analysis were studied with simple rules in which there are decisions involving if a cell is *dead* or *alive* [23, 52, 121]. We base our proposed model on that of Almaguer et al. [4], where a one-dimensional cellular automaton reproduce qualitatively the behavior of flocculation for wastewater treatment. The present work proposes an extension of this model into a multi-dimensional model. An exhaustive parameter-space exploration is presented and the results show that the proposed multi-dimensional extension improves the qualitative and quantitative agreement with actual jar-test experiments in a more robust manner.

## 1.1 HYPOTHESIS

It is possible to model the coalescence-fragmentation process based on jar-test apparatus data with an efficient computational model.

## 1.2 OBJECTIVE

Capture the coalescence-fragmentation process using three approaches; two computational: a cellular automaton model based on a previous approach in one-dimensional to a generalized version for any dimension and an urn model, and one theoretical: a differential equation model. Each approach associates variables that capture the fragmentation process, the coalescence process, and the experimental parameters: chemical concentration and agitation velocity.

## 1.3 STRUCTURE OF THE THESIS

The remainder of the thesis is organized as follows: Chapter 2 presents the background of theoretical concepts used in the elaboration of this thesis: coalescence-fragmentation process, cellular automaton, Markovian models, and differential equations. Chapter 3 describes a literature review relative to our problem, including different alternatives using simulated, mathematical, or theoretical approaches of the coalescence-fragmentation process. Chapter 4 describes the laboratory experiments of heavy-metal flocculation that the model seeks to reproduce. Also, the mathematical formulation of the proposed models is described. Chapter 5 discusses the implementation of the model and the numerical experiments performed with

---

the original and the proposed cellular automaton. Finally, Chapter 6 concludes the present work and discusses directions for future work.

## CHAPTER 2

# BACKGROUND

---

In this chapter we define basic concepts to be used in Chapter 4 where we explain our problem based on the case of study. First, in Section 2.1 the concepts of the case of the study (wastewater treatment) are presented. Also, the theoretical explanation of the principal process present in wastewater treatment, called coalescence-fragmentation process, is presented along with the explanation of physical process. Then, in Section 2.2 the general view of the most common methods used to explain a physical phenomena or similar situations are presented as we seek to reproduce the behavior of the coalescence-fragmentation process. After that, we introduce the basic theory behind of our proposed numerical approaches. Finally, the definition of the specific characteristics in the methodologies are presented.

## 2.1 WASTEWATER TREATMENT

The wastewater treatment process depends on the location due to the equipment of the industry, the chemicals present in the wastewater and others, but the basic steps of process of treatment occur in the same order. We structure the wastewater treatment in the following four phases:

1. **Coagulation-Flocculation:** In this step, a chemical (polymer or other) is added to untreated wastewater. Upon mixing, the particles start to coagulate (stick together). Next, the groups of coagulated particles start to form larger and heavier particles called *flocs*. These flocs are easy to remove from the wastewater once the mixing has concluded.
2. **Sedimentation:** Due to the floc-formation progress, the flocs start to settle in the bottom of the recipient (i.e., tank).
3. **Filtration:** Several minutes after the sedimentation, the water flows to a filter specially designed to remove the formed flocs depending on their sizes. Usually, in the industry, the filters are made of layers of sand and gravel. In laboratory tests the filters are paper layers.
4. **Disinfection:** The treated water is cleaned by collecting the suspended flocs. On the other hand, if the flocs are dangerous to the environment, the residual flocs are maintained and handed over to the environmental companies that can take care of them.

In this work, we focus on the first step (coagulation-flocculation process), but as we have no access to industry data, we base our work on an experimental process conducted with laboratory equipment that replicates the basic steps of the wastewater treatment to perform the analysis. The experimental process is called *jar test* that consists in mixing chemicals with a wastewater-industry sample in jars and performing an external agitation, taking samples each minute to determine the floc-size distribution. We focus on the shape of the floc-size distribution of the experiment. Our proposal uses differential equations, cellular automaton theory, and urn models based in Markovian theory to understand the behavior of the process. In the next sections, an explanation of these methods is provided.

### 2.1.1 COALESCENCE-FRAGMENTATION PROCESS

The principal step of treatment wastewater is the coalescence-fragmentation process where the heavy-metal particles form *flocs* (larger particles) that are easier to remove. In the absence of external agitation, gravitational force will, over time, result in sedimentation on the bottom of the recipient. Without agitation, the particles are less probable to collide and join together to form larger flocs. Flocs of size from 0.001 and 1 micrometers are often called *colloids*.

The principal objective of the coagulation process is to permit the surface of the floc to be able to accept more particles in order to grow. This mechanism is ideal for the removal of the formed flocs by filtration or sedimentation. Also, this process is considered a chemical treatment, because it makes the particles unstable (more able to join with others) by changing the electrical charges of the particles.

The suspended colloids and particles that have not been sedimented are of special interest. These have a negative charge that makes the particles and colloids to repel, thus unable to join them. So, the purpose of a *coagulant* is to neutralize the surface charge. This allows particles to join together and form flocs that are easier to remove. The usual coagulant is the aluminum sulfate  $\text{Al}_2(\text{SO})_3 \cdot 18\text{H}_2\text{O}$ , although other coagulants, such as  $\text{FeCl}_3$  and  $\text{FeSO}_4$ , can also be used.

Basically, by adding the coagulant, the wastewater is ionized (changing its charge to positive) and the ions of the coagulant neutralize the charges of the colloids. The ions react with the water and form hydroxides that are insoluble. The hydroxides create conglomerates that absorb unstable particles. The unstable particles can also aggregate and grow through collision between themselves (i.e., those that are not yet sedimented). The destabilization grade is measured by *collision efficiency factor*  $\alpha$ , the quantity of collisions result in aggregation. If the particles are completely

unstable, all the collisions result in aggregation ( $\alpha = 1$ ), meanwhile if  $\alpha = 0.25$ , a quarter of the collisions end in aggregation.

In the industry, coagulants are added in the wastewater in a tank with external agitation by paddle. The usual time of agitation in the tank is less than one minute. But, the *flocculation* (process in which the colloids or particles collide to form the flocs), continues with a gentle agitation for half an hour. During this period of time, the hydroxide precipitates in a floc. The mixing in the flocculation tank needs to be done carefully and has to be fast enough to promote the collision between flocs so that they to grow in size, but not too fast because the colisions can break the flocs. The mixing provokes the contrary effect of the sedimentation where the particles have more opportunity to interact [83].

The agitation level on the tank is denotated by  $G$ , the intensity of the mixing; it is the parameter used to maximize the collision rate between particles. The intensity of mixing  $G$  depends on the energy applied to the rotational arms,

$$G = \sqrt{\frac{P}{\mu V_b}}, \quad (2.1)$$

where  $P$  is the energy used for the rotation (or whichever other mixed system),  $V_b$  is the volume of the tank, and  $\mu$  is the viscosity of the water. As the intensity of mixing  $G$  increases, a *turbulent flow* (the regime in which the fluid flows is chaotic and present changes in pressure and flow velocity) is achieved. Otherwise, if the intensity of mixing  $G$  decreases, a *laminar flow* (the regime which occurs when a fluid flows in linear parallel layers) is achieved.

The agitation rate can be represented by the change of concentration of the flocs. The concentration of the flocs  $n$ , where single particles or aggregated in flocs exists, are obtained dividing by the volume. Every time two particles collide to form

a floc, the concentration decreases. So the velocity of flocculation can be represented mathematically in terms of  $dn/dt$ .

The coalescence-fragmentation process theory is extensive, so we present only the part relevant to our problem. To comprehend the process we use simple assumptions: all the particles are the same size (*monodisperse distribution*), every particle has the shape of a sphere, the mixing of the water is soft (*laminar mixing*), and the volume of aggregates flocs is the sum of individual particles that form them (coalescence). In this case, the flocculation velocity (change rate) can be expressed by:

$$r(n) = -kn, \quad (2.2)$$

where

$$k = \frac{\alpha 4VG}{\pi}, \quad (2.3)$$

$\alpha$  is the collision efficiency factor, mentioned previously,  $V$  is the volume of the floc assuming that is spherical is defined by

$$V = \frac{\pi d_p^3 n_0}{6}, \quad (2.4)$$

where  $n_0$  is the initial number of monodisperse-particles concentration with a diameter  $d_p$ . The volume of the floc can also be represented by the total volume of solids per volume of water, in other words, the volume of particle concentration. The total volume of flocs is constant as the flocs are simply rearrangements of the existing particles — no new particles arrive and none disappear — but the number of individual flocs at any given time may vary due to the aggregation process.

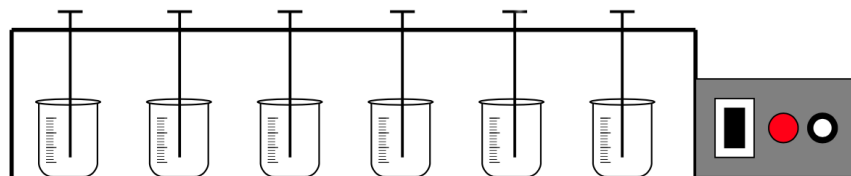


Figure 2.1: Typical setup of a jar-test apparatus.

### 2.1.2 JAR-TEST APPARATUS

The purpose of the jar test is to select different types of coagulants, estimate the ideal conditions of dosage and agitation speed to remove the heavy-metal particles from wastewater. The jar test helps understand the behavior of coalescence-fragmentation process in the laboratory. Performing all the experimentation in the industry leads to high costs and it may even be necessary to interrupt the operation of a plant to carry out experiments.

Usually, the *jar-test apparatus* consists in six jars of one liter each, equipped with a paddle mixer. The paddle mixer allows to move the fluid so the particles can interact, regulating the agitation speed. Also, the equipment controls the agitation speed, with a rotor that moves the paddle. A sketch of a typical jar-test apparatus is shown in Figure 2.1.

The principal steps of the jar test are adding coagulant to the wastewater, mixing rapidly to homogenize, followed by slow agitation to promote the collisions that form the large flocs, and finally the sedimentation process to remove the formed flocs. We are interested in the step where the slow agitation is performed because the flocs are formed at that point. Also, we focus on the interactions that form the flocs.

To start the test, a wastewater sample is placed in each jar (see Figure 2.2a). Then, a chemical is added, usually sodium hydroxide, to raise the pH of the disso-

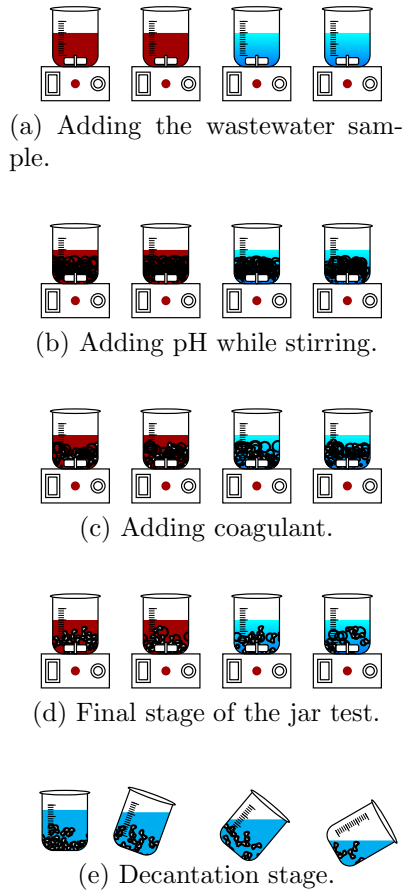


Figure 2.2: The principal steps of the jar test.

lution until a certain pH is reached (i.e.,  $\text{pH} = 10$ ), while stirring at a fast agitation speed (see Figure 2.2b); this depends on the specification of the jar-test apparatus (i.e., 150 rpm). Next, the coagulant is added (see Figure 2.2c) and the agitation speed is decreased until a slow agitation (i.e., 20 rpm) is reached. In this step the pH is neutralized again to  $\text{pH} = 10$ . The coagulant solutions are prepared using the salts. During the agitation, a sample of 10 mL is obtained every minute, put in a filter, and left to dry. Usually, the duration of agitation is about half an hour. When the agitation is finished, the mixture is left to permit the separation of the particles (see Figure 2.2d). Finally, the mixture is decanted (see Figure 2.2e) to separate the flocs.

## 2.2 MATHEMATICAL MODELS

Since the XI century, it is accepted that nature is governed by mathematical laws. In the beginning of the XX century, the researchers use mathematical laws to describe and explain some phenomena under certain conditions (restrictions by the observer), and feasibility of the solution [6].

A *mathematical model* uses mathematics to express the relationship between variables, parameters, entities to study behaviors of complex systems under situations that are difficult to observe systems in the real world. There are different classifications of the models according to their input information, representation, randomness, or application [38].

The input information can be based on: explanations about causes and natural mechanisms (*heuristic model*), or direct observations of an experiment of the studied phenomena (*empiric model*).

The figures, graphics, or descriptions are used to represent the mathematical model to predict in which direction the system is going. The description in which a value is decreasing or increasing without any information is called a *qualitative model*, or if the change of a value is described with formulas and mathematical algorithms the description is called *quantitative model*.

The randomness in the model can happen if the result is always the same as the data used has no variations (*deterministic*), or if the result is unknown and only the probability of some aspects of the process are known (*stochastic*).

A final aspect in which models can differ is their application. Three types are *simulation* that describes measured situations in a precise or a random way in order

to predict what happens in a concrete situation, *optimization* to solve a problem by obtaining the exact value that meets the requirements and structure of the problem, and *control* to help to determine new measures, variables or parameters in order to improve the results of the system.

The *simulation of a process* consists in the representation of a process or phenomena with a logic-mathematical model capturing its particular behavior [57]. It is a useful tool in the engineering, because of the detailed description that is capable to show for a process. Some types of simulations can be modeled using discrete events, agents theory, or differential equations [44, 61, 79].

In the following sections, we present different approaches to model the behavior of a process through the variations of some property in the process. Also, we include the basic theory to understand the dynamics and uncertainty of a process.

### 2.2.1 DIFFERENTIAL EQUATIONS

A *differential equation* is a mathematical equation that describes the change of a variable  $y$  respect to another variable  $x$ . Usually, the equation is represented by the derivative of a function  $y$  that depends on  $x$  or another variables. In some applications, the function represents physical quantities like heat or temperature. In these cases, a derivative represents the rate of change of the quantity, and the equation describes the relation between the variables. Because of the capability to describe the relationship between two or more variables, differential equations have been used in different disciplines such as engineering, physics, economics, and biology, among others, as a main tool.

Differential equations are studied for different reasons, but the majority of

the application of such models focus on their solutions (the set of conditions or functions that satisfy the equation). If the differential equation is simple, it can be solvable by an explicit formula, but in many cases the use of an explicit formula cannot obtain the exact solution or even determine if there is a solution. Hence, when no analytical solution is available, computational implementations of numerical methods are applied [7].

Here, the main problem is to determine how many segments of the independent variable  $x$  need to be taken into account. If there are too few segments, the evolution of the dependent variable  $y$  is not described correctly. To solve differential equations, many numerical methods have been developed over time. Method selection depends on the structure of the differential equation, because of the degree of accuracy reached by the methods. Even with all the information available on find a solution other methodologies to solve some differential equations are required. In these cases, it is necessary to make simplifications but always seeking to represent with the highest possible amount of detail.

If the case of study is a process that variate over the time as in a phenomenological process, the typical simplification is to treat the time  $t$  as a discrete interval. First, time  $t$  starts with the value zero. Then, an increment  $\Delta t$  is applied to increase the value of the variable. That is repeated until the interval is covered as  $t$  reaches the maximum desired value.

### 2.2.2 STOCHASTIC PROCESSES

*Probability theory* is a field that initiated with two French mathematicians, Blaise Pascal and Pierre de Fermat, in the XVII century, and remains an active research area today. Since then, many applications and discussion of the probabilistic theory

have gained importance in the world. The different applications include computer programming, physics, chemistry, music, whether forecasting, and medicine, among others.

Probability theory is a branch of the mathematics that describes and calculates the likelihood of an event occurs, expressed as a number between zero (impossible) and one (certain). To describe probability in numbers, take the event of tossing a coin where the possible results are *heads* or *tails*. A probability equal to one implies that an event always occurs: for example, the probability that a coin toss result in *heads* or *tails*, because there are no other options. A probability equal to one half implies that an event is equally probable to occur; for example, the probability of a coin toss result in *heads* is 0.5, on the other hand, the probability on resulting *tails* is equally probable than to result in *heads*. A probability equal to zero implies that the event cannot occur; for example, the coin lands in another result that is neither *heads* nor *tails*, which is impossible because the coin only has two sides.

Also, with probability theory it is possible to measure the uncertainty of a random event using precise calculations. The simple way to represent probability mathematically is dividing the number of occurrences (success  $a$ ) of a targeted event by the total number of possible outcomes (successes  $a$  and failures  $b$ ) of that event:

$$p(a) = \frac{f(a)}{f(a) + f(b)}. \quad (2.5)$$

For a coin toss, the computation of the probability is simple, because the outcomes are *mutually exclusive*: only one event, *heads* or *tails*, can occur. Also, each coin toss is an *independent event*: the outcome of a toss does not rely on the previous toss. No matter how many consecutive outcomes of a single result occur, the probability of the result of the next toss is always 0.5 for either *heads* or *tails*.

In the following sections, we present formulations of two methodologies that use probabilistic theory: cellular automaton theory and urn models. These two methodologies are used to describe complex systems or processes using simple assumptions. Specifically, the process of our interest (coalescence-fragmentation process) is complex to model due to the number of flocs in the system and the interactions between them. We believe that using these two methodologies, the most important characteristics of the coalescence-fragmentation process, and taking into account the nature of the process, the behavior of the real process can be accurately captured.

### 2.2.3 CELLULAR AUTOMATON THEORY

The *cellular automaton* was presented for the first time in the 1940's by Stanislaw Ulam and John Von Neumann. It became interesting to academia in 1970 with Conway's Game of Life, followed by Wolfram [122] in the 1980's, and since then has been studied and researched by many others due to its capacity to obtain information with simple models and rules; the analysis of the characteristics [60], the applicability in areas like equilibrium physics, chemical reactions, population dynamics and parallel computers [62], generation of signals [84], the study of connections between dynamical and computational properties [37], the study on new paradigms for improvement in computational using quantum devices [74, 85], the structure and topology [9], the evolution of the cellular automaton in disorder states [88, 103], and configuration [125], among others modeling and simulating some complex macroscopic phenomena.

A cellular automaton is a mathematical structure that models dynamic systems composed of arrays of cells that evolve their state following local rules that are applied globally. The evolution process is carried out in discrete steps. The cellular automaton is used to model and simulates natural systems or complex macroscopic

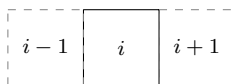


Figure 2.3: Von Neumann neighborhood for a one-dimensional automaton.

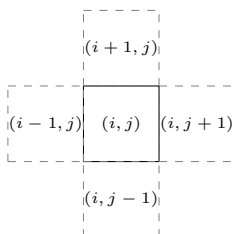


Figure 2.4: Von Neumann neighborhood for a two-dimensional automaton.

phenomena [35] with huge amount of objects (cells, particles, flocs, etc.) interacting locally with each other following rules [122], represents an alternative approach to the classical with partial differential equations, and it consists in the following considerations:

- A *dimension*  $d$  in which the cellular automaton exists.
- A  $d$ -dimensional  $n$ -cell lattice space, where the lattice coordinates are a vector with  $d$  elements.
- Each cell is denoted by an index  $c$  and characterized by its *neighborhood*, a finite set of cells in its vicinity. Different structures of the neighborhood exist: one of the most used is the Von Neumann neighborhood (see Figure 2.3 for one-dimensional and Figure 2.4 for two-dimensional automaton) that consists in all the cells that differ in exactly one lattice coordinate from the cell  $c$ . If the lattice coordinates differ in more than one coordinate, it is not considered a neighbor. No cell is considered its own neighbor.
- The lattice coordinates also can be of different types depending on boundary condition. One condition is called *regular lattice*; for example, in two-dimensional automaton, cells at the four corners of the lattice only have two

(0, 3)	(1, 3)	(2, 3)	(3, 3)
(0, 2)	(1, 2)	(2, 2)	(3, 2)
(0, 1)	(1, 1)	(2, 1)	(3, 1)
(0, 0)	(1, 0)	(2, 0)	(3, 0)

Figure 2.5: An example of a two-dimensional regular Cellular Automaton.

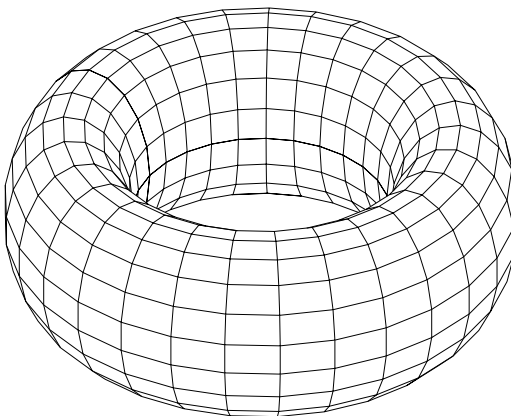


Figure 2.6: An example of a two-dimensional borderless Cellular Automaton.

neighbors and the cells along the four borders only have three neighbors (see Figure 2.5). The other one is called *borderless lattice*; the first cell in each dimension  $d$  is adjacent with the last cell (see Figure 2.6). There are more neighborhoods but these two are the most commonly used in the literature.

- A set of *local rules* (also called a *transition function*) that governs the change of each cell  $c$  between the current state of the automaton and the next state.
- A discrete *global clock* that provides homogeneously an update signal for all cells.

### 2.2.4 URN MODEL

The *urn model* is used to illustrate the basic ideas of probabilistic theory in many textbooks [97, 108, 117]. The usual examples presented in the textbooks deal with balls of different colors that fill urns, then the balls are randomly drawn from a selected urn. The typical questions are: how many draws are required to draw a ball of specific color, what is the probability of drawing two balls of specific color, what is the chance that in the  $i$ -th draw a ball of specific color is drawn, etc.

Urn models are easy to understand, so a variety of situations can be expressed with these models. Some experiments of games of chance, such as coin tossing and dice rolling, can be rearranged into urn models.

An urn model is represented by a set of  $n$  urns containing  $m$  balls of different colors  $c$ . To represent the number of balls of a color in a urn  $c_m$  is normally used. The typical experiment is when the balls, according to some rules, are removed from one or more urns but can be replaced or not depending on the experiment. Usually when a ball is drawn from a urn, the probability to be chosen is the same for every ball in the urn.

When an urn model is analyzed, the variables of interest are:

- the distribution of balls of various colors at the  $i$ -th draw,
- the number of balls of a certain color obtained after the  $i$ -th draw,
- the waiting time until a specific condition is reached, for example, how many time until is draw the  $i$ -th ball of the urn?

Some examples of the most basic urn models are presented next:

- An urn contains  $a$  white balls and  $b$  black balls,  $n$  balls are drawn at random from the urn. The balls can or cannot be replaced after each draw. Examples of events are: obtain a white ball in the first extraction, obtain a black ball in the second extraction, etc; typical questions are: obtain the probability of certain event, or what is the probability that in the fifth extraction to draw a white ball.
- A teacher has a desk with two drawers. The first drawer contains  $a$  red pens and  $b$  blue pens. The second one has  $c$  red pens and  $d$  blue pens. Typical questions are: if a drawer is opened at random and a pen is drawn, find the probability of that pen is red, or if a blue pen is drawn what is the probability that it came from the second drawer?

The urn models are also used to capture the behavior of phenomena where interactions between its entities are present. In order to capture the phenomenon, it is used urns to represent its states, balls to represent its entities, and the movement of a ball between urns to represent the changes of the state that allows to determine the distribution of the entities between states [31, 45, 112]. This distribution is one of the interesting characteristics of certain phenomena like in the coalescence-fragmentation process where the floc-size distribution is the principal objective.

## CHAPTER 3

# LITERATURE REVIEW

---

In this chapter we present a literature review relevant to the coalescence-fragmentation process. This process is an important phenomenon that has been studied to understand its behavior due to the presence of such a process in many applications such as colloidal chemistry, polymer science, magnetic nanoparticles suspensions, and wastewater treatment [40, 63, 102, 115, 119]. Theoretical models are the first approaches that attempt to reproduce the coalescence-fragmentation process in order to understand its behavior. In the following sections, a review of the theoretical models, the balance equation, the laboratory analysis, the application in wastewater, approaches using cellular automaton techniques, and other similar process that behave similarity to the coalescence-fragmentation process are presented. In the literature sometimes coalescence is referred as aggregation and fragmentation is referred as break-up.

### 3.1 COALESCENCE-FRAGMENTATION PROCESS

There are many approaches to model the coalescence-fragmentation process. The first approaches use a discrete, deterministic model which can be traced back to

the work of Smoluchowski [104] and as well as Becker and Döring [14]. Since these studies, several characteristics and solutions of the model have been studied providing a detailed information of what happens with the microscopic and macroscopic interactions present in the coalescence-fragmentation process. Family et al. [42] generalize the standard coalescence-fragmentation process including the effects of fragmentation and develop a scaling description for floc-size distribution using the Smoluchowski rate equation to obtain the critical exponents describing the steady-state floc-size distribution with numerical simulation to test the predictions of the scaling and the rate equation.

The solution of the equation presented by Smoluchowski [104] became of interest as it permits to better understand the behavior of the coalescence-fragmentation process. Elminyawi et al. [40] numerically solve the Smoluchowski rate equation for different combinations of coalescence and fragmentation kernels observing the long-term equilibrium size, the characteristic time to reach the equilibrium and the floc-size distribution. Bohin et al. [15] present experimental and theoretical results for dispersion agglomerates, developing a model for the kinetics of the homogeneous sparse of the agglomerates. To test the model, Bohin et al. [15] use agglomerates of silica to demonstrate the mechanism, kinetics rates of dispersion, and floc-size distribution. Broizat [21] formulate a theorem that uses compactness methods in  $L^p$ -norms propagation (mathematical function of spaces for a finite-dimensional vector), the natural physical bound, and assumptions of finite number of flocs in the kinetic model of coalescence-fragmentation. Banasiak and Lamb [11] prove the unique solution of the coalescence-fragmentation equation introducing coalescence and fragmentation rates. The proof is based on a monotonicity argument of the invariance for the fragmentation.

Also, the study of inclusion of external forces began to gain interest. Collier

and Hounslow [32] examine the relation between the growth and coalescence rates as a function of the agitation rate, initial concentrations, and use a stirrer speed with five speeds. Soos et al. [106] propose an approach based on measurement and quantitative modeling of multiple moments of the floc mass distribution. They apply this model to coalescence processes in turbulent conditions in order to test alternative kernels for coalescence, fragmentation, and restructuring kinetics.

Another works implement in a practical application. Winterwerp [120] presents a three-dimensional model for the evolution of the *settling velocity* (velocity required to settle the flocs to the bottom of a liquid and form a sediment) of estuarine mud resulting in coalescence and fragmentation processes. The mud flocs are treated as *fractal* (geometric irregular object that repeats in different scales) entities. Also, a new formula is proposed which account for the gelling process typical of cohesive sediment at high concentrations. Kumar et al. [70] investigate the flocculation properties of a natural silt-clay mud observing a range of suspended sediments concentrations, salinities, and turbulent shear rates. They use a paddle mixer to create a turbulent sheared field for driving the flocculation process. They measure the floc settling velocity and size attributes in a settling column with a camera system and image analysis. They observe maximum floc sizes in *sheared rates* (rates at which a progressive deformation due to collision is applied to flocs) less than  $30 \text{ s}^{-1}$ . It is suggested that this variability in *fractal dimension* (i.e., an index for characterizing fractal patterns or sets by quantifying their complexity as a ratio their change in detail to the change in scale) may physically be the result of many different floc sizes of *primary particles*. Primary particles refers to particles which can affiliate to a larger linked system such as flocs.

Recently, some important characteristic of the solutions have been determined, such as the moments of a distribution; including mean and variance. Manning and

Dyer [81] describe a new flocculation model based on observations of the settling floc and turbulent agitation acquired from experiments conducted in European estuaries. They identify the change in the macro-floc and micro-floc settling as the key components that describe a floc population. Banasiak [10] studies discrete coalescence-fragmentation equations in a space where a distribution has finite moments, shows by simply fragmentation rules the equations can be analyzed and characterized. The results obtained by Banasiak [10] show the existence of solutions for the unbounded coalescence kernels. Also, Banasiak and Lamb [12] use a large range fragmentation rates to show that the continuous fragmentation operators are sectorial and prove the solution of the coalescence-fragmentation equation with unbounded coalescence kernels.

## 3.2 COALESCENCE PROCESS

The coalescence process is also of interest in applications where the particle interactions end in a group of particles with larger sizes that are easily to handle. The particles that group are called *aggregates*. Brasil et al. [19] present a procedure to characterize the proprieties, structural and fractal, of aggregates from a projected images. From the images, they determine the particle diameter, maximum projected length, projected area, and overlap coefficient. The data they use is from simulations of aggregates that has fractal properties and primary particles to characterize three-dimensional properties of aggregates.

Later, Brasil et al. [20] investigate the structure of cluster-cluster and particle-cluster fractal-like aggregates. Also, they characterize the three-dimensional properties using statistically significant populations of simulated aggregates. The three-dimensional properties include the fractal dimension, fractal prefactor, coordination

number distribution function, and distribution of angles. They consider the effects of coalescence process and coalescence size. They use a coefficient for allow the flocs to approach each other, and also a process where two flocs join together and start to collapse when a stable size is achieved. Gmachowski [48] explores the fractal dimension when the structure of growing aggregations is scale invariant and conclude that the fractal dimension of an aggregate can be determined by the *radius of gyration*<sup>1</sup>. Mokhtari et al. [86] study the behavior the effect of low shear rates on a coalescence *colloidal* (microscopical disperse insoluble particles) systems made of polystyrene particles. They conclude that the slow shear can enhance the coalescence and gelation.

Xu et al. [123] study the influence of the *transport* of fine-gradient particles in estuarine and coastal waters by both flocculation processes coalescence and fragmentation. Here the floc size varies over time in the water column. They simulate the variations of floc size using *size-resolved* (flocs for which the particle sizes are known) method, which approximates the real size distribution of flocs. They use a constant *coalescence kernel* where the interactions are simplified by the collision rate in turbulent shear and *differential settling*<sup>2</sup>. Following the same approach, Xu et al. [124] implement a size-resolved flocculation model for an ocean circulation to simulate fine-grained particles trapping in a turbidity maximum. They include flocs of small sizes, about 30  $\mu\text{m}$ , to very large flocs, over 1 000  $\mu\text{m}$ . Also, they formulate a two-dimensional model to simulate variations of suspended sediment concentrations.

Zahnow et al. [127] study the steady-state floc-size distributions in a three-dimensional *synthetic turbulent flow* (generated velocity fluctuations that are close to turbulence) flow based on the dynamics of individual particles. They introduce effective densities and radius to capture the fractal-like structure in the coalescence

---

<sup>1</sup>The distribution of the components of an object around an axis; in this case the radial axis.

<sup>2</sup>Uneven floc sizes that sink during and after some time of a phenomenon with coalescence.

and fragmentation model. Specifically, they apply this methodology in marine aggregates in coastal areas. Three mode of fragmentation were studied: large-scale splitting (similar sizes in fragments), erosion (one fragment is smaller than the other), and uniform fragmentation (all sizes occur with the same probability).

### 3.3 POPULATION BALANCE EQUATION

The population balance equations are a set of integro-partial differential equations that have been used in many areas like chemical engineering since the 1960's because they are capable to represent the behavior of a population of flocs from the analysis of a single particle giving local conditions. Since then they are become one of the most important tools for design and control of particulate processes and so many studies have studied them [91].

Kumar and Ramkrishna [71] present a new framework to perform the discretion of the continuous population balance equations. The framework proposes that the discrete equation for coalescence or fragmentation process is consistent with the desired moment of the floc-size distribution. Also, they consider floc population to be concentrated at representative volumes. The technique is applicable to binary or multiple coalescence, fragmentation, simultaneous coalescence and fragmentation, and can be adapted to predict the desired properties of an evolving size distribution more precisely. Kumar and Ramkrishna [72] propose a discretization method to solve population balance in simultaneous nucleation, growth and coalescence of flocs. The features of the method are: properties of floc-size distribution, arbitrary grid control, computational efficiency. They tested the method in pure growth, simultaneous growth and coalescence, and simultaneous nucleation and growth. They analyze a large number of combinations by changing, nucleation rate, growth rate, coalescence

kernel and initial conditions. Verkoeijen et al. [113] propose a volume model based on population balance equation in which the floc properties are the volumes of solid, liquid, and air.

Flesch et al. [46] use a population balance equation to model coalescence-fragmentation process in turbulent shear. They quantified the fractal-like structure using a mass fractal dimension. They compare with experimental data (polystyrene- $\text{Al}(\text{OH})_3$ ) of a water system in a stirred tank with paddle mixers: the aggregate size increases before reaching a steady-state during the coalescence-fragmentation process. Ramkrishna and Mahoney [92] discuss the application of population balance modeling towards strengthening the approach as well as widening the application scope with regard to formulation, computational methods for solution, inverse problems, control of floc populations and stochastic modeling. Mahoney and Ramkrishna [78] evaluate the performance of two improvements of *Galerkin's method* [94] on finite elements to solve population balance equations for *precipitation systems*<sup>3</sup>. Qamar and Warnecke [90] propose two methods to solve population balance models with simultaneous nucleation, growth, and coalescence processes. The first method combines a method of characteristics for growth process with a *finite volume method*<sup>4</sup> for coalescence process. The second method uses purely a semi-discrete finite volume scheme for nucleation, growth and coalescence of flocs. Both schemes use the same finite volume scheme for coalescence process.

Meanwhile, Kumar et al. [68] develop a discretization method for population balance equations called cellular average technique. They assigns the particles to cells by taking first the average of the new particles within the cell and then as-

---

<sup>3</sup>Creation of a solid from a liquid solution with chemical when a reaction occurs. The solid formed is called the *precipitate* and the chemical that causes the solid to form is called the *precipitant*.

<sup>4</sup>A discretization technique for partial differential equations, especially those that arise from physical conservation laws.

signing them to the neighboring nodes such that pre-chosen properties are exactly preserved. The technique is useful for systems with a gelling point. Later, Kumar et al. [66] extend a cell average discretization to solve multi-dimensional population balance equations in diffusion processes. The method is based on the prediction of a certain moment of the population. Their methodology is simple to implement, computationally not expensive and highly accurate. Next, Kumar et al. [67] solve the population balance equation using the discretization for simultaneous coalescence, fragmentation, growth, and nucleation based on a *cell average technique* [68]. Finally, Kumar et al. [69] compare the results of two different approaches to solve the population balance equation. The first one is the proposed by Kumar et al. [67] based on a cell average technique and the second one is a finite volume method.

Waldner et al. [116] monitor a stirred tank with coalescence kinetics of colloidal polymeric particles in diluted dispersion. They apply a population balance model in the early stage when the fragmentation is in lesser proportion than the coalescence. They determine analytically the coalescence rate and the effective fractal dimension for aggregates produced by the initial growth regime. Soos et al. [107] study the coalescence and fragmentation process for destabilized polystyrene latex particles under turbulent flow. They use an optical image technique to monitor the process. They use population balance equations to study the process and compare with experimental. They observe the evolution of the floc-size distribution, seeking to capture the small flocs and large aggregates. Rollié et al. [96] simulate coalescence of nanoparticles in binary particle mixtures using a population balance models in terms of their coordinates. Parameter sensitivity with respect to the fractal dimension, aggregate size, hydrodynamic correction, ionic strength, and absolute floc concentration are assessed.

### 3.4 FLOC DISTRIBUTION

Hill and Ng [56] propose a procedure to target the floc-size distribution using a functional structure and the discretion of the population equations to determine the feasibility. They illustrate this procedure in three examples: the production of salt, alumina, and metronidazole tablets. Li et al. [76] perform numerical simulations to determine the floc-size distribution in marine waters by accounting for floc influx, coagulation, sedimentation and fragmentation. They state that a steady state in the floc-size distribution can be achieved after a period of simulation regardless of the initial conditions and follows a *power-law*<sup>5</sup> function with three linear regions on log-log scale corresponding to the three collision mechanisms: Brownian motion, fluid shear, and differential sedimentation. They obtain that the environmental condition does not change the floc-size distribution but can modify the position and the concentrations of flocs.

Tansel and Sevimoglu [110] perform a investigation in the floc-size distribution of oil droplets after coagulation extension of the cell average technique. Al-Thyabat and Miles [3] propose a method to determine the floc-size distribution using the equivalent area and mean *Feret's diameter*<sup>6</sup>. Andres et al. [5] compare two techniques to an image analysis of spherical standard powders to determine the floc-size distribution. Ko and Shang [64] use a sensor with neural network based model and image analysis to determine the floc-size distribution. Cheng et al. [24] measure the turbidity of a mix with a turbidimeter coupled with data acquisition and obtain that the standard deviation of the turbidity was proportional to the square root of the floc size. Cheng et al. [24] use image analysis for validation.

---

<sup>5</sup>One quantity (bin size) varies as power of another (normalized frequency).

<sup>6</sup>A measure of an object size defined as the distance between two parallel tangential lines that restrict the object.

### 3.5 WASTEWATER TREATMENT APPLICATIONS

Jiang and Graham [58] investigate the behavior in the hydrolysis/precipitation of the poly-ferric sulfate and ferric sulfate under typical conditions for coagulation and flocculation in water treatment by studying the rate of floc-size development, the zeta potential, chemical structure of precipitates, and the *isoelectric point*<sup>7</sup> of re-suspended precipitates. Rossini et al. [98] study the parameters of rapid mixing (rapid dispersal of a coagulant into the raw water followed by an intense agitation) design: velocity gradient and rapid mixing time. They use aluminum (III) and iron (III) salts to treat the wastewater from a tannery processing stored. They determine an optimal combination of rapid mixing parameters and use the approaches for high turbid synthetic water obtained by suspending kaolin in distilled water to compare the results with tannery wastewater.

Bouyer et al. [17] investigate the coalescence-fragmentation process in water treatment units using jar-test vessel to analyze the hydrodynamics and floc-size distribution. The parameters that control are the water quality (pH) and the coagulant dose. Bouyer et al. [17] analyze the floc-size distributions by image processing. They determine the evolution on the floc-size distribution by statistical analysis that leads to velocity gradients. Battistoni et al. [13] present a physical-chemical pre-treatment in the treatment of liquid wastes, optimizing the flow scheme. Battistoni et al. [13] discuss the types, amount, and characteristics of the wastewater to reduce the use of strong oxidative treatments, obtaining a significant reduction of the solids. Ramphal and Sibiya [93] study the sizes and structural characteristics of floc in water treatment. They optimize the coagulation-flocculation parameters with a photometric dispersion analyzer coupled to standard jar test experiments while monitoring floc

---

<sup>7</sup>The pH where no net electrical charge of a particular molecule is carried.

size and structure of the floc formation during coagulation using alum. Data reveals that coalescence rate and steady-state variance are primary parameters as both have substantial influence on coagulation-flocculation efficiency.

### 3.6 LABORATORY ANALYSIS

Kang and Cleasby [59] study the effect of low water temperature on flocculation kinetics using ferric nitrate to coagulate kaolin clay in water. They measure the flocculation kinetics with floc-size distribution obtained by an automatic image analysis, and with on-line measurement of the degree of turbulence. Manning and Dyer [80] examine the turbulent shear generated water column is recognized as having a controlling influence over both the flocculation of fine grained cohesive sediments within estuary waters, and their respective coalescence or fragmentation. The use of algorithms which were based either on a single characteristic floc, size or settling velocity, or a mean fractal dimension, were seen not to accurately approximating the experimental data. A multiple regression analysis of the experimental data produced the following formula, based on mean values of the 20 largest flocs sampled under each of the imposed environmental conditions.

Franceschi et al. [47] study the behavior of the variation in different scales systems or same scale systems in the flocculation performances using different impeller geometries. Franceschi et al. [47] study the influence of raw water quality and operating conditions on the effectiveness of the coagulation-flocculation process using aluminum sulfate. Verney et al. [114] investigate the behavior of a floc population during a idealized radial cycle. They use suspended sediments at a small concentration (93 mg/ $\ell$ ). Also, they use a jar-test apparatus to reproduce tidal-induced turbulence and coupled with a Charge Coupled Device camera system and

image post-processing software to monitor floc-size distribution and developed a model based on the coalescence-fragmentation process to simulate changes in the floc population over the tidal cycle.

### 3.7 CELLULAR AUTOMATON

Grinstein et al. [50] study the conditions of a probabilistic cellular automaton arguing in that with irreversible rules, continuous ferromagnetic transitions in probabilistic cellular automaton with *up-down* symmetry. Also a non-stationary states are achieved for asymptotically large time by certain probabilistic cellular automaton rules. Seybold et al. [100] use a two-dimensional asynchronous cellular automaton that simulates both the deterministic and the stochastic features of a first-order chemical kinetic processes to avoid the numerical solution of either the deterministic coupled differential rate equations or the stochastic master equation. They found that deterministic solutions emerge as statistical averages in the limit of large cell numbers and examine some additional stochastic and statistical features of the solutions that they obtain. Nowak [87] study a microscopic mechanism of grain size dependence of creep using simulation of damage development done by cellular automaton technique. Almaguer et al. [4] present a one-dimensional cellular automaton that capture the essential of the coalescence-fragmentation process and is the base of our model. Yan et al. [126] model the growth and coalescence of multiple cracks in brittle material with a continuous-discontinuous cellular automaton. The method uses the level set to track arbitrary discontinuities, and calculation grids are independent of the discontinuities and no remeshing are required with the crack growing. A mixed fracture criterion for multiple cracks growth in brittle material is proposed to treat the junction and coalescence of multiple cracks.

The lattice Boltzmann method which belongs to the cellular automaton techniques is widely used to study the dynamics of fluids in physical phenomena Perumal and Dass [89]. Higuera and Jimenez [55] propose an alternative simulation for lattice hydrodynamics based on lattice Boltzmann model instead of on the microdynamics evolution. They simplify the method averaging the step and the associated fluctuations, and selecting the collision operator independent of a particular collision rule to decrease viscosity as much as desired. Ernst et al. [41] study the lattice gases equation of Boltzmann comparing theoretical and molecular dynamics. Somers [105] study turbulent flow using hexagonal lattices gas given a balance between robustness and numerical accuracy with three-dimensional time-dependent flows in turbulent flows. Cieplak [30] study the coalescence-fragmentation process in two liquid systems using a two-dimensional non-linear, *Galilean invariant*<sup>8</sup>, and lattice Boltzmann cellular automaton. They characterize the dynamics of rupture with parameters such as the coefficient of the surface tension. The case study is a droplet in a gravitational field to the bottom of a container. Three cases (a bare wall, a shallow liquid, and a deeper liquid) are studied.

Di Gregorio et al. [36] apply a cellular automaton model to represent the dynamics of spatially extended physical systems instead of the classical partial differential approach. They simulate the bio-remediation of contaminated soils. The model is hierarchical and composed by a fluid dynamical layer, a solute description layer, and a biological layer. They test the model in a pilot plan when there are contamination by phenol. They use genetic algorithms to determine the values of the phenomenological parameters. They prove that the model describe experimental results in a wide range of experimental conditions. Therefore, their model represents an example of an application of the cellular automaton in a real-world problem which has a very high social and economic importance. D'ambrosio et al. [33] use a cellular

---

<sup>8</sup>The laws of physics are the same in all inertial frames of reference.

automaton to model the soil erosion by water including the states altitude, water depth, total head, vegetation density, infiltration, erosion, sediment transport, and deposition. They perform a simulation and apply the model in an actual water reservoir. Haslam et al. [53] model the deformation of a porous solid through which fluid flow. They show an initial proof of concept for a coupling method solving one-dimensional and multi-dimensional diffusion problems.

Chopard and Masselot [28] combine the cellular automaton and lattice Boltzmann to describe a system where point-flocs are transported in a fluid; the cases of studies are: snow transport, erosion, and deposition by wind. Next, Chopard and Luthi [27] discuss the connection between lattice Boltzmann computing and cellular automaton and present a model to simulate propagation in complex environments. To illustrate the behavior of the new model, they present three applications: wave propagation in a city, solid body motion, and fracture phenomena. Chopard et al. [29] simulate erosion, deposition, and floc transport in a streaming fluid with a simple lattice gas model. The fluid is described by standard lattice Boltzmann model and the granular suspension by a multi-floc cellular automaton. They perform field measurements to compare with the prediction obtained by the model. The case of study is the ripples formation and simulation of the scour appearing around a submarine pipe. Later, Chopard and Dupuis [26] use the combination of cellular automaton and lattice Boltzmann to model erosion processes in air or water currents, emphasizing on explaining the formation of meanders in rivers.

Korner et al. [65] use the lattice Boltzmann method to formulate a two-dimensional model that allows the investigation of the foam evolution process comprising bubble expansion, bubble coalescence, drainage, and foam collapse. Gupta and Kumar [51] use a lattice Boltzmann method to understand the behavior of a bub-

ble motion and bubble coalescence in liquid. The *drag coefficient*<sup>9</sup> for single bubble motion under buoyancy for both two-dimensional and three-dimensional simulations compares well with existing correlations. For multiple bubbles, the bubble dynamics is dictated by the vortex pattern of the leading bubble, which allows the bubbles to coalesce. Coalescence can be described as a three stage process: collision, drainage of the liquid film between adjacent bubbles to a critical thickness, and rupture of this thin film of liquid.

### 3.8 OTHER SIMILAR PROCESSES

The following literature review introduces to some interesting similar processes of the coalescence-fragmentation process. Ahsan and Alaerts [1] describe a mathematical model for gravel bed in horizontal flow. The model was based on the parallel palette settler where the sedimentation and flocculation processes occur. Boisvert et al. [16] explore other areas where the process exist like the adsorption of mono-phosphate from aqueous solutions where the flocs are formed upon hydrolysis of alum ( $\text{Al}_2(\text{SO})_3$ ) and basic alum (poly-aluminum-silicate-sulfate), a coagulant is added and the pH is adjusted to promote the adsorption. They focus on the floc formed resistant to shear stress. Dzwinel et al. [39] propose a homogeneous computational model for performing numerical experiments on liquids employing three types of simulation techniques: molecular dynamics, dissipative floc dynamics and smoothed floc hydrodynamics. Boyle et al. [18] present an experimental analysis on the hydrodynamic forces involved in two types of dispersion regimes were examined, unfiltered and partial filtered structures where the process occurs in spherical agglomerate dispersion. They demonstrate the infiltration for silica agglomerates to different extends by the suspended fluid.

---

<sup>9</sup>An a-dimensional quantity to represent the resistance of an object in a fluid environment.

Al-Tarazi et al. [2] develop a mathematical model to describe the precipitation process of metal sulfides in aqueous solutions containing two different heavy metal ions where the solution is assumed well-mixed. Their model includes the transfer of gaseous hydrogen sulfide  $H_2S$  that is model using *Higbie's penetration model* [54]. The conditions in the simulations are similar to those of industrial wastewater from a zinc factory. Their model predicts the rate of  $H_2S$  absorption, the size distribution of the metal sulfide crystals, and the selectivity of precipitation. Another study on precipitation is presented by Lewis [75] who reviews the disparate areas of study into metal sulfide precipitation. The review includes studies that focus on mechanisms of the processes and very low concentrations, applied studies on metal removal and reaction kinetics, studies that focus on the solid phase and address the crystallization kinetics of the formed flocs, studies into precipitation of metal sulfide nanocrystals, and applications of metal sulfide precipitation to effluent treatment processes.

### 3.9 DISCUSSION

The presented literature review covers some aspects of the phenomenology of the physical-chemistry process called coalescence-fragmentation process. There are mathematical formulations of the floc interactions using differential equations or integro-differential equations, also the transformation of these formulations into a discrete models to reduce the tractability are performed, others use stochastic models to reduce the interactions between flocs. Nevertheless, the reviews leave neglected the comparison between experimental data and their models, and the statistical validation and reproduction of the model in order to capture the behavior of the coalescence-fragmentation process or similar processes.

We seek to capture similar characteristics that are studied in the reviewed lit-

erature to reliably reproduce them for our case study of wastewater heavy-metal removal in a jar-test apparatus. Our main interest lies in the coalescence-fragmentation process. The characteristics of interest are the floc-size distribution, interactions between flocs, and the ability to reproduce some states like the gelation state of the model or steady states in which the flocs reach sizes to easy remove them. Our model introduces a basic feature of a global instability threshold  $\bar{h}^*$  that can be interpreted as a physical constant that acts on all of the flocs in the system, similar to those used in models for sandpiles [8], earthquakes [77, 82] and fracture of materials [43]. To our knowledge, only Almaguer et al. [4] adds such a mechanism in their one-dimensional automaton but they are only able to capture some parts of the floc-size distribution in some state and did not validated their model. We validate our model with the analysis of the solutions obtained by Wattis [118] and a new proposed differential equation models that use the global instability threshold  $h^*$  to simplify the interactions between flocs. The choice of a macroscopic automaton is motivated by the goal to simulate large-scale systems. We perform an extensive analysis of the parameters to better adjust our multi-dimensional model to the experimental data. Also, we are able to reproduce the temporal evolution of floc of larger sizes that are easy to remove as in the laboratory experiments.

## CHAPTER 4

# METHODOLOGY

---

In this chapter, we discuss the methodology of the thesis. In particular, we describe the laboratory data for the case study of removing heavy metals from wastewater with a coalescence-fragmentation process, controlling the agitation time and speed. This data is our baseline against which the proposed models are compared, as we seek to precisely capture the behavior of the process in the laboratory.

First, in Section 4.1, we describe the data and how it was obtained as well as its statistical characteristics. Next, in Sections 4.2.1, 4.2.2, and 4.3 we propose three mathematical models for the coalescence-fragmentation process. The first model is a numerical approach that involves differential equations based on the coalescence-fragmentation process described in Chapter 2. The second model is the generalization of a one-dimensional cellular automaton described by Almaguer et al. [4]. The third model is a novel approach with Markovian analysis using an urn model.

## 4.1 CASE STUDY: WASTEWATER REMOVAL

The industry wastewater with presence of heavy-metal floc is an issue of human health [109]. Inadequate treatment of industrial sludge results in contamination of rivers, oceans, and drinking water sources that represents a danger to the ecosystem. Nevertheless, in some developing countries, the industry generates large amounts of poorly treated wastewater because of the lack of regulations for environmental care [22, 101]. Hence the removal of heavy-metal flocs that is both efficient and cost-effective is important [101, 109].

We focus our work on the removal of heavy metals through coalescence and fragmentation controlling agitation time and speed. The experimental data is from a *jar-test apparatus* (see Figure 2.1), where controlling a rotor moving a paddle regulates the agitation speed (a timer to control the agitation time is also included) and the samples are placed into the jars to commence the treatment. The test sample is based on the typical chemical composition of galvanic-industry wastewater. A concentrated solution is used to prepare the treatment dissolution. First, to start the heavy-metals removal process, sodium hydroxide is added to raise the pH of the dissolution until a  $\text{pH} = 10$  is reached, while stirring at 150 rpm.

Next, a coagulant substance is added and the agitation speed is decreased to either 20 or 40 rpm, depending on the adjusted parameters of the test. The pH is neutralized again to  $\text{pH} = 10$ . The solutions are prepared using salts of either zinc chloride — Zn(II) at concentration of 750 mg/L — or iron chloride — Fe(III) at concentration of 200 mg/L — in one liter of distilled water.

Two data sets from a jar-test apparatus are considered. The first data set is from Almaguer et al. [4]. The second data set is from a laboratory experimentation

of longer duration than the first data set to observe when the particles start to aggregate, and also when the fragmentation process begins, as our analysis of the first data set indicates that the latter does not occur in most of that data.

**Data Set 1:** A two-level factorial design was carried out, using the salt (zinc versus iron) and the agitation speed (20 versus 40 rpm) as the two factors. Three replicas were conducted for each of the four combinations. The total agitation time for each experiment was set to ten minutes.

**Data Set 2:** A single experiment was carried out, using the iron salt and the agitation speed 25 rpm. One single replica was conducted. The total agitation time for the experiment was set to thirty minutes.

For both sets, every minute a sample of 10 mL was obtained and left to dry. After that an optical microscope<sup>1</sup> was used to measure the floc-size distribution in the sample. The distribution is quantified in terms of bins of five units each, determined by the laboratory equipment, the first bin being 10–15 due to lack of sensitivity. Examples of the obtained images are given for the first and the second data set in Figures 4.1 and 4.2, respectively. In both cases, several large flocs emerge after a period of constant agitation. This effect is desirable as the presence of large flocs promotes sedimentation and thus facilitates the removal.

The equipment has a minimum agitation speed of 5 rpm and a maximum agitation speed of 150 rpm. We carried out initial experiments with different agitation speeds in this range. When the agitation is too fast (higher than 120 rpm) the fragmentation begins to dominate and only small flocs form. If the agitation is too slow (less than 20 rpm) the coalescence becomes scarce and no relevant floc formation is

---

<sup>1</sup>Brand: Olympus, Model: BX60F5.

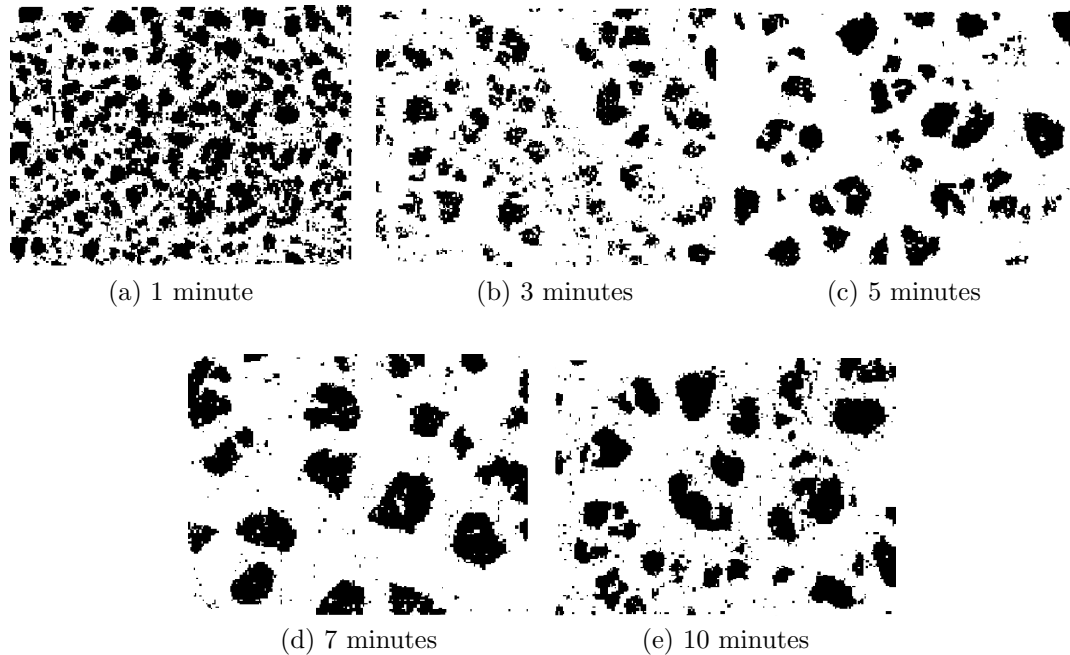


Figure 4.1: Microscopic images of the flocculation process, for the data set 1, observed at five different agitation times for iron chloride at an agitation speed of 20 rpm.

appreciated during the first 10 minutes but instead several hours are required for interesting behavior to emerge.

Each microscopy image sample from each minute is processed using a computational vision methodology in order to obtain the laboratory floc-size distribution. First, the image is transformed to its monochromatic version: we interpret white pixels as background and use the number of black pixels as a measure of floc size. Next, for each black area in the image (adjacent black pixels), the number of black pixels in the image is computed to do a depth-first search; when all the black areas are identified, we estimate the floc-size distribution for each sample. We consider that the ideal scenario for the easy removal of the flocs occurs when there are many flocs larger than fifty micrometers. In microscopic images, fifty micrometers is equal to forty-one pixels. The computer-vision method records the absolute frequencies that are then normalized to relative frequency.

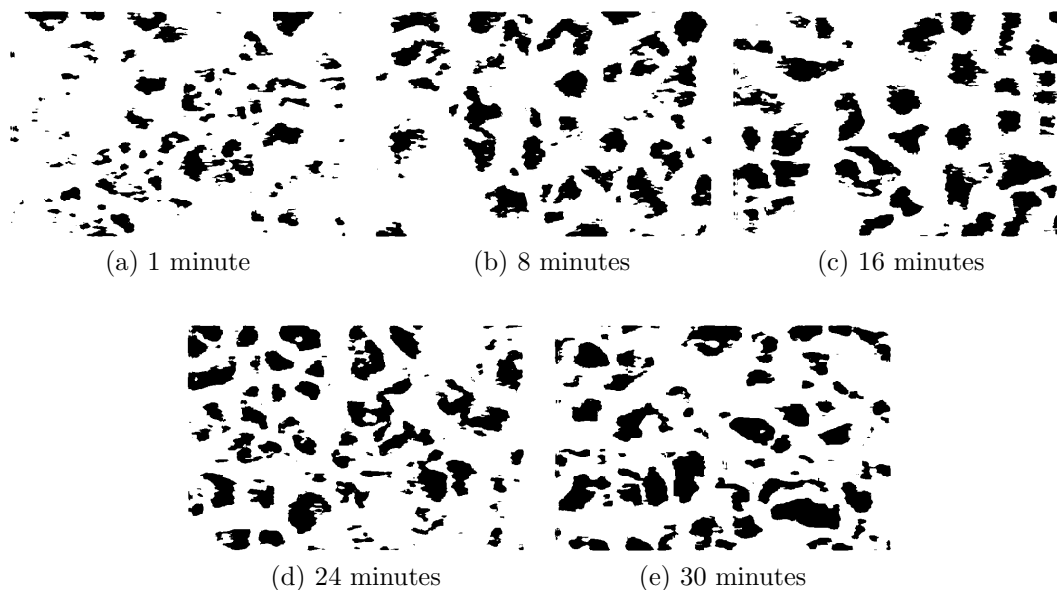


Figure 4.2: Microscopic images of the flocculation process, for the data set 2, observed at five different agitation times for iron chloride at an agitation speed of 25 rpm.

We are interested in floc-size distributions where the frequency of floc-size is a function of the floc size that gives rise to a power-law shape. This behavior is seen in the laboratory floc-size distributions (see Figure 4.3). In a power law, a straight line with a good fit appears on a plot of one quantity in the  $x$  axis (the floc size) versus other quantity in  $y$  axis (the normalized frequency), both in logarithmic scale. Therefore, we perform a linear regression on log-log plots to determine the *goodness of fit* in term of  $R^2$  (how good the fitted line explains the floc-size distribution) and the exponent of the power law (i.e. the slope of the fitted line). Once the goodness of fit is obtained, we can determine the presence of a power law and its shape.

Also, we are interested in shapes of the distributions with negative values (closer to zero) of slope because these values are observed in the laboratory floc-size distribution of all experiments where large flocs are present to easily remove them (see Figure 4.3). As not all agitation speeds leads to large flocs, the shape of the power-law shape of the floc-size distribution is restricted to certain forms and

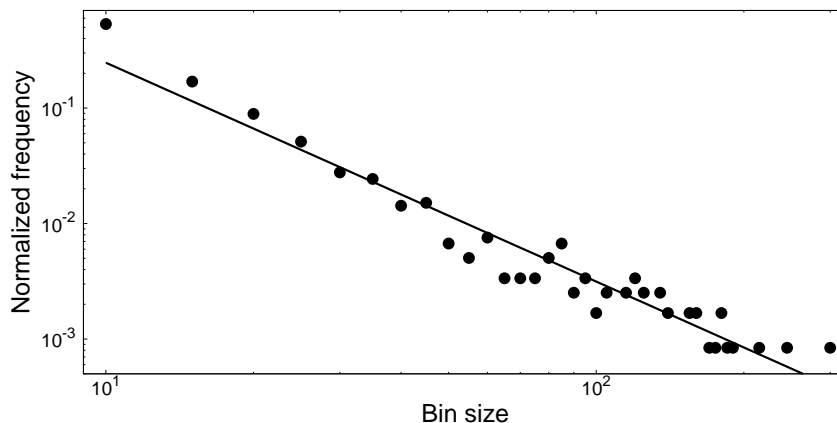


Figure 4.3: Experimental floc-size distribution for iron chloride at an agitation speed of 40 rpm after seven minutes of agitation. Both axes are in logarithmic scale.

negative values of the slope.

An example of the power-law shape from a floc-size distribution of the first data set in the seventh minute of the experiment showed in the microscopy images of Figure 4.1 is given in Figure 4.3 with  $R^2$  is 0.92 and the slope is  $-2.57$ .

## 4.2 PROBABILISTIC MODELS

In this section, we formulate a multi-dimensional extension of the one-dimensional automaton of Almaguer et al. [4] and a novel urn model that are based on the behavior of the coalescence-fragmentation process. For each model, the relevant concepts, considerations, and parameters are described. For the automaton, we discuss initial conditions, rules of interaction, and stopping criteria. For the urn model, the probabilistic models for coalescence and fragmentation are presented.

### 4.2.1 MULTI-DIMENSIONAL CELLULAR-AUTOMATON MODEL

The proposed automaton is an  $n$ -cell  $d$ -dimensional lattice with two types of border conditions — cyclic<sup>2</sup> or regular<sup>3</sup> — and the cell coordinates are represented as  $d$ -element integer vectors. Two cells are neighbors if and only if their coordinate vectors differ by exactly one unit in exactly one position.

An integer-valued state variable  $h_c$  is assigned to represent the floc size at each cell  $c$  of the lattice. The units that form the flocs are called *particles*. To initialize the automaton, a total of  $m$  particles in the  $n$  cells of the lattice are placed, resulting in an average floc size  $\bar{h} = m/n$ .

The rules, adapted from Almaguer et al. [4], govern the change of each cell  $c$  between the current state and the next state of the automaton. These rules are specified in terms of the floc size  $h_c$  of each cell, the average floc size  $\bar{h}$  (stability *threshold* to model the critic size that is when the flocs start the fragmentation process), a coalescence rate  $f$  (to model the solution), and a fragmentation rate  $v$  (to model the agitation speed). To provide an homogeneous update for all cells, we rely on a discrete *global clock*, giving rise to synchronous behavior. The primary unit of the clock is called *step*. Therefore, the evolution of the automaton is carried out step by step until a certain step is reached. The visual representation for a two-dimensional model in a steady state is given in Figure 4.4.

The parameter  $v$  represents floc *instability*: when  $v \rightarrow 1$ , only flocs of sizes below or equal to the average floc size  $\bar{h}$  are stable. The parameter  $f$ , on the other hand, represents floc *stabilization*: floc growth depends on  $f$  when  $v < 1$ . Our threshold is chosen based on the following experimental observation: with fast agitation, highly

---

<sup>2</sup>For example, in a one-dimensional automaton, the first cell is adjacent with the last cell.

<sup>3</sup>For example in two-dimensional automaton, cells at the four corners of the lattice only have two neighbors and the cells along the four borders that are not corner cells have three neighbors.

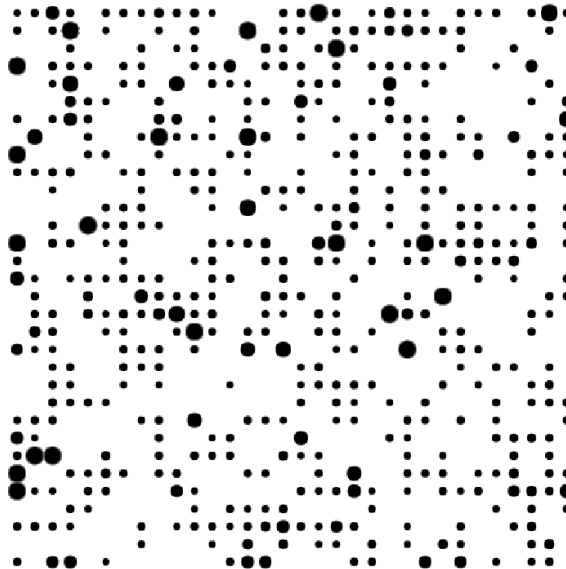


Figure 4.4: A visualization of a stationary state of a two-dimensional automaton. The area of each dot is linearly proportional to the floc-size of the cell.

stable flocs of minimal mesoscopic sizes dominate. From the assumption of mass conservation, the threshold being defined in terms of the average floc size  $\bar{h}$  follows from  $v = 1$  corresponding to the maximum agitation speed.

In the following sections the initial conditions, and the update schemes for the automaton are described.

#### 4.2.1.1 INITIAL CONDITIONS

Different initial conditions were implemented for the automaton, among which we chose one for each experiment. Detailed analysis of the impact of initial conditions are left to future work. We proceed to describe the initial conditions. The condition is named with the word *init* before the number. The description for each initial condition is presented next.

- init<sub>1</sub>**: Place uniformly at random a total of  $m$  particles in the  $n$  cells of the lattice, resulting in an average floc size  $\bar{h} = m/n$ .
- init<sub>2</sub>**: Place  $k$  particles in each cell  $c$ , resulting in an average floc size  $\bar{h} = k$ .
- init<sub>3</sub>**: Place at each cell  $c$  a number of particles chosen uniformly at random between zero and ten.
- init<sub>4</sub>**: First, set the average floc size  $\bar{h}$  and the total number of cells  $n$ . Then, the total particles  $m$  are obtained by multiplying the average floc size with the total  $n$  cells given by  $m = \bar{h}n$ . Next, for each particle a cell  $c$  is chosen at random from the  $n$  cells to receive one particle, repeating until all particles have been assigned to a cell.
- init<sub>5</sub>**: For each cell, draw the number of particles to be placed at that cell at random according to the laboratory-obtained floc-size distribution.
- init<sub>6</sub>**: Load the floc size at each cell from a saved state of the automaton.

#### 4.2.1.2 UPDATE SCHEMES

The update schemes of the cellular automaton are based on a discrete global clock that provides homogeneously an update signal for all cells: at each step all cells update their states *synchronously* (an update of each cell to a new state depends on a previous state of all its neighbors cells) or *asynchronously* (an update of a cell to a new state impact all its neighbors cells in the previous state) according to the set of rules. We only consider the asynchronously update scheme for our experiments and leave to future experimentation the analysis of including the other update schemes. The description of the two update schemes of the cellular automaton are presented.

**ASYNCHRONOUS** At each step, each cell  $c$  updates asynchronously its receptions or transfers according to the Rules 1A and 2A, the state variable  $h_c$  of the cell  $c$ , and its neighbors in the present state. The asynchronous update scheme is performed in such a way that the new state of a cell  $c$  affects the calculation of states in neighboring cells of the cell  $c$  itself.

**Rule 1A:** if  $h_c \leq \bar{h}$  then, with probability  $v$ , cell  $c$  *absorbs* the  $[\bar{h}] - h_c$  *excess* of each of its neighbors.

**Rule 2A:** if  $h_c > \bar{h}$  then, with probability  $f \cdot (1 - v)$ , the cell  $c$  *absorb* all the particles of all of its neighbors (as in Rule 1A); otherwise the cell *transfers* a fraction uniformly at random of its  $[\bar{h}] - h_c$  *excess* particles, choosing the receptor cell uniformly at random among its neighbors.

**SYNCHRONOUS** According to the Rules 1S and 2S, first each cell  $c$  prepares by scheduling its receptions and transfers according to the values of the state variables of the cell itself and its neighbors in the present state, after which the schedules receptions and transfers are executed, thus updating the state variables for the next state.

**Rule 1S:** if  $h_c \leq \bar{h}$  then, with probability  $v$ , cell  $c$  schedules an *absorption* of all the particles of all of its neighbors.

**Rule 2S:** if  $h_c > \bar{h}$  then, with probability  $f \cdot (1 - v)$ , the cell  $c$  schedules receptions (as in Rule 1S); otherwise the cell schedules for *transfer* each of its  $[\bar{h}] - h_c$  *excess* particles, choosing the receptor cell for each particle independently and uniformly at random among its neighbors.

Any transfer decisions are canceled if the transferring cell's particles are schedules for absorption by a neighboring cell.

For any of the update schemes, at the end of the simulation, the absolute floc-size distribution is obtained and normalized into a relative floc-size distribution. In order to be consistent with laboratory data that no record of flocs below size 10 due to lack of sensitivity of the equipment, we can strip the smallest flocs from the simulated distributions. The initial bin includes the floc sizes from 10 to 15. In the automaton, the smaller flocs (flocs with a floc-size less than 10) exist, but there are not included in the floc-size distribution to be consistent with the laboratory data.

We observe in our initial experiments that using the average floc size  $\bar{h}$  leads to poor results, meanwhile using the average floc size calculated in the local neighborhood of cell  $c$  improve the behavior. We leave to future exploration the results of the comparison between the global average floc size  $\bar{h}$  and the neighborhood average floc size. We also leave as future work an alternative implementation of the Rules 1A and 2A: first each cell mark its state as a *idle* (do nothing), *receptor* (wiling to receive particles), or *donor* (share particles). Last, the donors examine their neighbors share an even part of their excess particles and calculate how many receptors do they have and share an even part of its particles to each neighbor that is a receptor. The receptors do not actively absorb, but instead passively receive from the donors.

### 4.2.2 URN MODEL

Our proposed urn model has an urn for each floc size (technically from one to infinity, but in a practical implementations only the floc sizes present in the system need to be stored). We denote the number of flocs of size  $u$  by  $\rho_u$ . The update rules for the urns are formulated in terms of a threshold  $h^*$ , a fragmentation parameter  $\varphi$ , and a fragmentation parameter  $\xi$ . The threshold  $h^*$  is a parameter that can be set to any value; we propose  $h^* = \bar{h}$ , i.e., using the average floc size as a stability threshold.

Note that the parameter  $\varphi$  has a function similar to that of  $v$  in the automaton, whereas  $\xi$  acts similar to  $f$ . The initialization of the urn model can be done with different methods as in the cellular automaton: i.e., place a total of  $m$  number of particles into the urn of floc-size one, or create  $n$  urns and place particles uniformly at random in each urn  $u$  yielding the initial value of  $\rho_u$ . The rules are as follows:

**Fragmentation Rule:** Each floc of size  $u$  breaks into two with probability  $p_f(u, \varphi)$

$$p_f = 1 + \exp\left(-\frac{u - h^*}{\varphi}\right). \quad (4.1)$$

Equation (4.1) has the shape of a sigmoid function (see Figure 4.5). The sizes of the two resulting flocs are uniformly distributed (although this distribution may also be varied to alter the behavior of the model).

**Coalescence Rule:** Each floc of size  $u$  joins an aggregation list with probability  $p_a(u, \xi, s)$ , where  $s$  is the fraction of remaining salt

$$p_a = \xi s \exp(-su). \quad (4.2)$$

Equation (4.2) has the shape of an exponential distribution (see Figure 4.6). The pairs are drawn uniformly at random of the aggregation list that combines the flocs of all sizes that entered the list. Each pair is joined into a new larger floc and a salt is consumed. When no more salt is available, the aggregation ceases. Each aggregate between two flocs consumes a unit of salt. Any flocs remaining in the aggregation list after the salt runs out are returned to their original urns.

Experiments with this model are left to future work, although our initial tests show promise in terms of precision, flexibility, and efficiency.

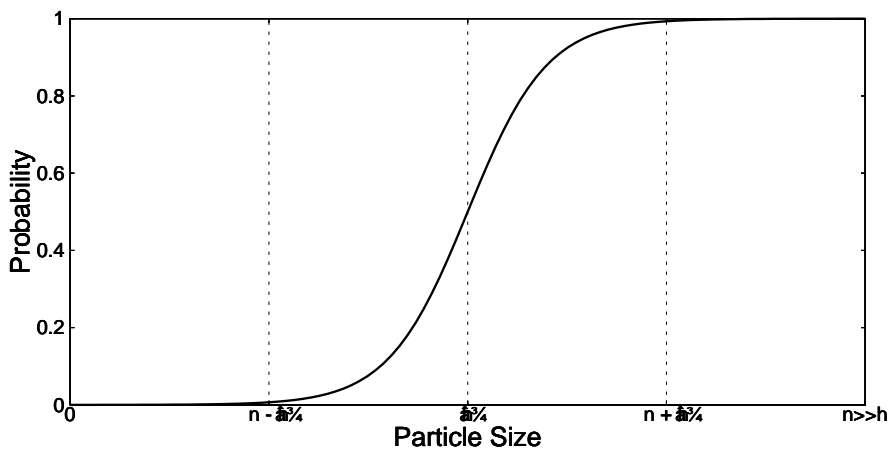


Figure 4.5: Example of a sigmoid function.

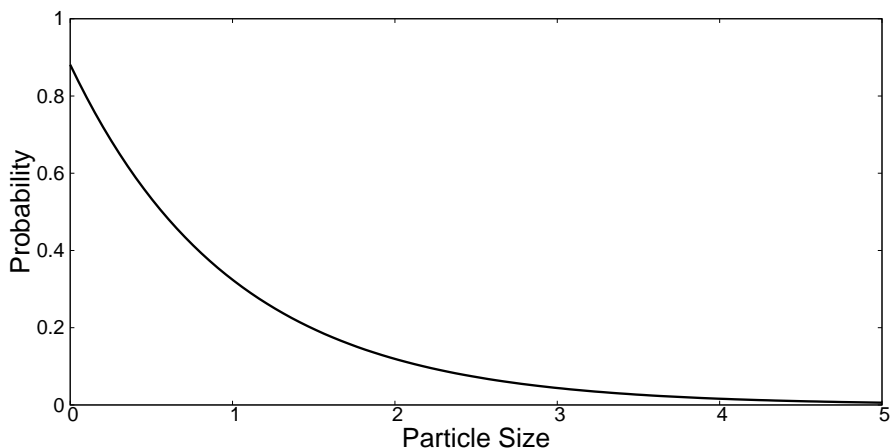


Figure 4.6: Example of an exponential distribution.

### 4.3 DIFFERENTIAL EQUATION MODEL

The proposed differential equation model is based in the behavior of the coalescence-fragmentation process when a external force is added. The expected behavior is that the flocs<sup>4</sup> above a *stable size* are unstable and can be fragmented. If the flocs are below a stable size only coalescence of flocs can occur. This behavior is represented in our model using the stable size  $h^*$ . If a floc of size  $n$  is above  $h^*$  can be separated into two flocs of sizes  $i$  and  $j$ , being one of them barely closer to the stable size  $h^*$ .

<sup>4</sup>The flocs are clusters of size  $n$  being  $n$  the number of particles.

The fracture is similar to the microscopic behavior where the floc of size  $n$  transfers its *excess* from  $h^*$ . We assume that the stable size  $h^*$  in the differential equation model represents the average floc size  $\bar{h}$  although it could take on arbitrary values.

The inclusion of the stable size  $h^*$  simplifies the fragmentation  $F$  and coalescence  $A$  terms of the Smoluchowski-type model as Equation (1.1) on page 2. In order to include multi-particle exchanges that are present in the general Smoluchowski equation, it is necessary to include two regimens in terms of the stable size  $h^*$ :

$$\begin{aligned} & n = i + j > h^* : & (4.3) \\ \frac{d\rho_n}{dt} &= \frac{1}{2} \sum_{i+j=n} A_{i,j} \rho_i \rho_j - \sum_{j=1}^{\infty} A_{n,j} \rho_n \rho_j - \frac{F}{2} \rho_n + F \rho_{n+h^*}. \\ & n = i + j \leq h^* : \\ \frac{d\rho_n}{dt} &= \frac{1}{2} \sum_{i+j=n} A_{i,j} \rho_i \rho_j - \sum_{j=1}^{\infty} A_{n,j} \rho_n \rho_j. \end{aligned}$$

Equation (4.3) is a Smoluchowski-type balance equation and describes the evolution of the density of a *floc*  $\rho_n$  according to the densities  $\rho_i$  and a stable size  $h^*$ . The coalescence kernel  $A_{ij}$  is the reaction rate for an aggregation of a floc size  $i$  floc with a floc size  $j$ , and the fragmentation kernel  $F$  is the constant reaction that simplify the interactions of floc sizes  $i$  and  $j$ . In both regimes, the multiplier  $\frac{1}{2}$  is included to eliminate double counting the interactions of floc sizes  $i$  and  $j$  (for example,  $1+2=3$  and  $2+1=3$  for  $n=3$ ).

The combinatorial and exponential growth of Equation (4.3) persist on the coalescence rate but not in the fragmentation rate as the interactions of flocs are canceled with the inclusion of the stable size  $h^*$ . To simplify the coalescence interactions between flocs, the separability of the densities  $\rho$  on Equation (4.3) and two assumptions on the coalescence rate are considered.

### 4.3.1 CONSTANT COALESCENCE RATE

The first assumption used to simplify the model of Equation (4.3) is that the coalescence rate is constant  $A_{i,j} = A$ , yielding

$$\begin{aligned} n = i + j > h^* : \quad (4.4) \\ \frac{d\rho_n}{dt} = \frac{1}{2}A \sum_{j=1}^{n-1} \rho_j \rho_{n-j} - A \sum_{j=1}^{\infty} \rho_n \rho_j - \frac{F}{2}\rho_n + F\rho_{n+h^*}, \\ n = i + j \leq h^* : \\ \frac{d\rho_n}{dt} = \frac{1}{2}A \sum_{j=1}^{n-1} \rho_j \rho_{n-j} - A \sum_{j=1}^{\infty} \rho_n \rho_j. \end{aligned}$$

The system of couple ordinary differential equations in Equation (4.4) can be represented as single partial differential Equation (4.5) using a transformation ( $Z$ -transform) with a generating function  $\hat{\rho}(z, t) = \sum_{n=1}^{\infty} \rho_n(t)z^{-n}$

$$\frac{\partial \hat{\rho}(z, t)}{\partial t} = \frac{A}{2}\hat{\rho}^2(z, t) - \hat{\rho}(z, t) \left[ A\hat{\rho}(1, t) + \frac{F}{2}(1 - 2z^{h^*}) \right] - F \sum_{j=1}^{h^*-1} \rho_j z^{h^*-j}. \quad (4.5)$$

The solution of Equation (4.5) admits stationary solutions,

$$\hat{\rho}(z) = \hat{\rho}(1) + \frac{F}{2A}(1 - 2z^{h^*}) \pm \frac{1}{2} \sqrt{\left[ 2\hat{\rho}(1) + \frac{F}{A}(1 - 2z^{h^*}) \right]^2 + 8 \left( \frac{F}{A} \right) \sum_{j=1}^{h^*-1} \rho_j z^{h^*-j}} \quad (4.6)$$

where

$$\hat{\rho}(1, t) = \frac{F}{2A} \pm \frac{1}{2} \sqrt{\left( \frac{F}{A} \right)^2 - 8 \left( \frac{F}{A} \right) \sum_{j=1}^{h^*-1} \rho_j}, \quad (4.7)$$

is the total number of flocs in the system.

In the stationary regime of Equation (4.5), a normalization factor  $1/\hat{\rho}(1)$  and the derivatives of the characteristic function are used to obtain the first two moments

— mean  $\langle n \rangle$  represented by Equation (4.9) and variance  $\langle n(n+1) \rangle$  represented by Equation (4.9) — of the stationary floc-size distribution:

$$\langle n \rangle = \frac{-1}{\hat{\rho}(1)} \frac{d\hat{\rho}}{dz} \Big|_{z=1}, \quad (4.8)$$

$$\langle n(n+1) \rangle = \frac{1}{\hat{\rho}(1)} \frac{d^2\hat{\rho}}{dz^2} \Big|_{z=1}. \quad (4.9)$$

Applying Equations (4.9) and (4.9) into Equation (4.5) result in a closed system:

$$\begin{aligned} -A\hat{\rho}(1) \langle n \rangle + \langle n \rangle \left[ A\hat{\rho}(1) - \frac{F}{2} \right] + Fh^* - \frac{F}{\hat{\rho}(1)} \sum_{j=1}^{h^*-1} (h^* - j)\rho_j &= 0, \quad (4.10) \\ A\hat{\rho}(1) \langle n(n+1) \rangle + A\hat{\rho}(1) \langle n \rangle^2 - 2Fh^* \langle n \rangle \\ - \langle n(n+1) \rangle \left[ A\hat{\rho}(1) - \frac{F}{2} \right] + [Fh^*(h^* - 1)] \\ - \frac{F}{\hat{\rho}(1)} \sum_{j=1}^{h^*-1} (h^* - j)(h^* - j - 1)\rho_j &= 0. \end{aligned}$$

Isolating the two moments on the closed system in Equation (4.10), we obtain

$$\begin{aligned} \frac{1}{2} \langle n \rangle &= h^* - \frac{1}{\hat{\rho}(1)} \sum_{j=1}^{h^*-1} (h^* - j)\rho_j, \quad (4.11) \\ \frac{1}{2} \langle n(n+1) \rangle &= 2\langle n \rangle h^* - \frac{A}{F} \hat{\rho}(1) \langle n \rangle^2 - h^*(h^* - 1) \\ &\quad + \frac{1}{\hat{\rho}(1)} \sum_{j=1}^{h^*-1} (h^* - j)(h^* - j - 1)\rho_j. \end{aligned}$$

We introduce auxiliary notations

$$\alpha \equiv \frac{1}{\hat{\rho}(1)} \sum_{j=1}^{h^*-1} \rho_j, \quad (4.12)$$

$$\beta \equiv \frac{1}{\hat{\rho}(1)} \sum_{j=1}^{h^*-1} j\rho_j, \quad (4.13)$$

$$\gamma \equiv \frac{1}{\hat{\rho}(1)} \sum_{j=1}^{h^*-1} j^2\rho_j \quad (4.14)$$

in order to express Equation (4.11) as

$$\begin{aligned}\langle n \rangle &= \frac{h^*(1-\alpha)}{\frac{1}{2}-\beta}, \\ \langle n^2 \rangle (1-2\gamma) &= \langle n \rangle (4h^* - 1) - \frac{2A}{F} \hat{\rho}(1) \langle n \rangle^2 - 2h^*(h^* - 1) \\ &\quad + 2(\alpha h^{*2} - 2\beta h^* \langle n \rangle - \alpha h^* + \beta \langle n \rangle).\end{aligned}\tag{4.15}$$

The first two moments of the stationary floc-size distribution are defined in Equation (4.15) when  $0 < \alpha < 1$ ,  $0 < \beta < 1/2$ , and  $\gamma > 1/2$ . Also, the mean  $\langle n \rangle$  shows a linear growth in terms of  $h^*$  and the variance  $\langle n^2 \rangle$  shows a second-order polynomial growth in terms of  $h^*$ . If  $F/A$  is closer to zero but non zero, the mean and variance are large and diverge which correspond to the limit  $F/A \rightarrow 0$ ,  $\hat{\rho}(1) \rightarrow 0$ , and  $\beta \rightarrow 1/2$ . The presence of stationary state under these conditions occurs in finite time; to explain this behavior consider  $F/A \ll 1$  and the use of Equation (4.7),

$$\frac{F}{A} = \frac{1}{1 - \frac{2}{\alpha} \sum_{j=1}^{h^*-1} \rho_j}.\tag{4.16}$$

The consideration  $F/A \ll 1$  implies that the sum  $\sum_{j=1}^{h^*-1} \rho_j \ll \hat{\rho}(1, t)$ ,

$$\frac{d\hat{\rho}(1, t)}{dt} = -\frac{A}{2} \hat{\rho}^2(1, t) + \frac{F}{2} \hat{\rho}(1, t),\tag{4.17}$$

leading to

$$\hat{\rho}(1, t) = \frac{F}{A[1 - e^{-(\frac{F}{2})t}]}.\tag{4.18}$$

Therefore, a stationary state at  $F/A \ll 1$  with large mean and variance is obtained in the system described on Equation (4.11) under the time  $t_c \approx \frac{2}{F}$ . This kind of behavior is absent when pure coalescence model is considered, as a gelation transition occurs at infinite time; that is, the formation of a *superparticle*, also known as *gel*.

### 4.3.2 ADDITIVE AND MULTIPLICATIVE COALESCENCE RATES

The second assumption used to simplify the model of Equation (4.3) is that the coalescence rate  $A$  is additive  $A_{i,j} = A(i+j)/2$  or multiplicative  $A_{i,j} = Aij$ . The resulting system of equations for both additive and multiplicative are presented. The first two moments on the results of these systems are not defined, but however some important features of the stationary states can be derived.

First, the additive case  $A_{i,j} = A(i+j)/2$  leads to,

$$\begin{aligned} & n = i + j > h^* : \quad (4.19) \\ \frac{d\rho_n}{dt} &= \frac{An}{4} \sum_{j=1}^{n-1} \rho_j \rho_{n-j} - \frac{An\rho_n}{2} \sum_{j=1}^{\infty} \rho_j - \frac{A\rho_n}{2} \sum_{j=1}^{\infty} j\rho_j - \frac{F}{2}\rho_n + F\rho_{n+h^*}. \\ & n = i + j \leq h^* : \\ \frac{d\rho_n}{dt} &= \frac{A}{4} \sum_{i+j=n} (i+j)\rho_i\rho_j - \frac{A}{2} \sum_{j=1}^{\infty} (n+j)\rho_n\rho_j. \end{aligned}$$

The system of couple ordinary differential equations in Equation (4.19) can be represented as single partial differential Equation (4.20) using a transformation ( $Z$ -transform) with a generating function  $\hat{\rho}(z, t) = \sum_{n=1}^{\infty} \rho_n(t)z^{-n}$

$$\begin{aligned} \frac{\partial \hat{\rho}(z, t)}{\partial t} &= -\frac{A}{2}z\hat{\rho}(z, t)\frac{\partial \hat{\rho}(z, t)}{\partial z} + \frac{A}{2}z\hat{\rho}(1, t)\frac{\partial \hat{\rho}(z, t)}{\partial z} - \frac{A}{2}M_1(t)\hat{\rho}(z, t) \\ &\quad - \frac{F}{2}(1 - 2z^{h^*})\hat{\rho}(z, t) - F \sum_{j=1}^{h^*-1} \rho_j z^{h^*-j}, \end{aligned} \quad (4.20)$$

where  $M_1(t) \equiv \sum_{j=1}^{\infty} j\rho_j$  is the total mass of the system. Introducing the mean  $\langle n \rangle$  in Equation (4.20) leads into a stationary state defined as

$$\langle n \rangle = \frac{F}{A} \left[ 1 - 2 \left( \frac{\sum_{j=1}^{h^*-1} \rho_j}{\hat{\rho}(1)} \right) \right], \quad (4.21)$$

when the condition  $\hat{\rho}(1) > 2 \sum_{j=1}^{h^*-1} \rho_j$  is given.

Second, the multiplicative case  $A_{i,j} = Aij$  leads to

$$\begin{aligned} n = i + j > h^* : \\ \frac{d\rho_n}{dt} = \frac{1}{2} \sum_{i+j=n} ij\rho_i\rho_j - \sum_{j=1}^{\infty} nj\rho_n\rho_j - \frac{F}{2}\rho_n + F\rho_{n+h^*}, \\ n = i + j \leq h^* : \\ \frac{d\rho_n}{dt} = \frac{1}{2} \sum_{i+j=n} ij\rho_i\rho_j - \sum_{j=1}^{\infty} nj\rho_n\rho_j, \end{aligned} \quad (4.22)$$

with the associated single partial differential function,

$$\begin{aligned} \frac{\partial \hat{\rho}(z, t)}{\partial t} = \frac{A}{2} z^2 \left[ \frac{\partial \hat{\rho}(z, t)}{\partial z} \right]^2 + AzM_1(t) \frac{\partial \hat{\rho}(z, t)}{\partial z} \\ - \frac{F}{2} (1 - 2z^{h^*}) \hat{\rho}(z, t) - F \sum_{j=1}^{h^*-1} \rho_j z^{h^*-j}. \end{aligned} \quad (4.23)$$

The study of pure coalescence case ( $F = 0$ ) displays a number of interesting behaviors [118], but our interest lies in  $F > 0$  and the emerging stationary states. This behavior is obtained by introducing the definition of the mean  $\langle n \rangle$  into Equation (4.23),

$$\langle n \rangle = \sqrt{\frac{F \left[ \sum_{j=1}^{h^*-1} \rho_j - \frac{1}{2} \hat{\rho}(1) \right]}{A \hat{\rho}(1) \left[ \frac{1}{2} \hat{\rho}(1) - 1 \right]}}. \quad (4.24)$$

A stationary state of the floc-size distribution is shown in Equation (4.24) as the system is concentrated in a finite number of flocs constricted to the interval  $2 \leq \hat{\rho}(1) \leq 2(h^* - 1)$ .

## CHAPTER 5

# COMPUTATIONAL EXPERIMENTS

---

In this chapter, we discuss implementation of our cellular automaton model as well as the design and the results of computational experiments to validate, compare, and explore this implementation. First, in Section 5.1 the computational implementation of the cellular automaton is presented. Next, in Section 5.2 the experimental setup of the cellular automaton is presented. Later, in Section 5.2.1 the validation of our cellular automaton using the analysis and hypothesis of the Smoluchowski Equation presented by Wattis [118] and the analysis of our differential-equation model. After that, in Section 5.2.2 the comparison of our cellular automaton approach with the experimental data is shown. Finally, in Section 5.2.3 a large-scale exploration of the parameter space of the proposed multi-dimensional automaton is documented to characterize the relation between  $f$ ,  $v$ ,  $d$ , and the similarity between simulated and laboratory data.

## 5.1 IMPLEMENTATION OF THE CELLULAR AUTOMATON MODEL

The cellular automaton model is implemented in PYTHON<sup>1</sup> and executed using PYPY<sup>2</sup>. We analyzed and improved the efficiency by the implementation following the methodology presented by Gorelick and Ozsvald [49].

The model implementation allows for the dimension  $d \geq 1$  to take arbitrary integer values, but we restrict our reported experimentation to  $1 \leq d \leq 5$  as we saw little change in behavior as we increased the dimension further in our initial experiments.

We chose an object-oriented approach to implement the cellular automaton due to the nature where interactions between particles occurs. Each cell is an object with an unique label according to the order they are created. Also, the cellular automaton is an object that controls the cells. The total number of cells  $t$  is given as a parameter and  $k^{(1)} \times k^{(2)} \times \dots \times k^{(d)}$  regular lattice is formed where  $k^d$  is as close as possible to  $n$ .

The cellular automaton is represented with a PYTHON class. The input parameters are the total desired numbers of cells  $t$  and the dimension  $d$  for the automaton. The actual number of cells is obtained as  $n = \lceil \sqrt[d]{t} \rceil^d$  in order to have the same range of coordinates in all of the dimensions.

The objects representing cells are assigned unique numeric labels  $\ell = 0, 1, \dots, n-1$  and are stored in a dictionary object within the automaton. We use the rank and unrank functions provided in Algorithms Algorithm 1 and 2, respectively, to map be-

---

<sup>1</sup><http://www.python.org/>

<sup>2</sup><http://pypy.org/>

tween cell labels and their coordinate vectors, thus not having to store the coordinate vectors in memory.

---

**Algorithm 1** Label to Coordinates  $(\ell, d, k)$ 


---

```

1:  $\vec{c} \leftarrow \emptyset$ 
2:  $p \leftarrow k^{d-1}$ 
3: while  $p \geq 0$  do
4:    $i \leftarrow \ell/p$ 
5:    $\ell \leftarrow \ell - i * p$ 
6:    $\vec{c}_i \leftarrow i$ 
7: return  $\vec{c}$ 

```

---



---

**Algorithm 2** Coordinates to label  $(\vec{c}, d, k)$ 


---

```

1:  $\ell \leftarrow 0$ 
2:  $p \leftarrow k^{d-1}$ 
3: for  $i \in \vec{c}$  do
4:    $\ell \leftarrow \ell + i * p$ 
5:    $p \leftarrow p/k$ 
6: return  $\ell$ 

```

---

The simulation is initiated by a routine of the automaton class that receives as input the values for  $f$  and  $v$ , the number of steps to compute, and the number of replicas. Each replica is initiated in the same state. We initialize each cell with rule *init1* (see page 46) and the automaton computes  $m$  as the total number of particles over all of the cells, then computing  $\bar{h} = m/n$  and storing this constant as an attribute. The Rules 1A and 2A (see page 48) are implemented as subroutines of the cell. The implementation is available in a public repository at <https://luisbvzz@bitbucket.org/luisbvzz/proyecto-doctorado.git>.

## 5.2 EXPERIMENTAL SETUP

First, to validate our probabilistic cellular automaton, we chose the theoretical analysis of the Smoluchowski equation as represented by Equation (1.1) in page 2, for-

mulated by Wattis [118]. We set the step count high enough to reach the gel state (although this turned out to be impossible in the one-dimensional case). Our second experiment is a comparison of our one-dimensional case to the one-dimensional automaton of by Almaguer et al. [4].

Our final experiment consists in a parameter-space exploration to determine which values of  $f$  and  $v$  yield the best quantitative agreement with laboratory data, for which we propose a similarity measure to compare two steady states expressed in different units of time and size, as the laboratory data is in terms of minutes and pixel counts and the model data in terms of simulation steps and modeled floc sizes. Our proposed similarity measure is based on statistical properties of centrality and dispersion (captured by mean and standard deviation as the data mostly agrees with a normal distribution) of the relative proportion of large flocs after reaching the steady state. We use 50 micrometers as the threshold of a large floc for the laboratory data and a particle count of 50 for the simulation data, although the varying the values of the thresholds does not seem to alter the conclusions; we leave to future work a sensitivity analysis of adjustments to these thresholds.

Next, in Section 5.2 the experimental setup to *validate* our approaches is presented. After that, the *comparison* of our cellular automaton approach with the experimental data is shown. Finally, a large-scale *exploration* of the parameter space of the proposed multi-dimensional automaton is documented to characterize the relation between  $f$ ,  $v$ , and the similarity between simulated and laboratory data.

The execution of all experiments are on a computer with 8 Intel Xeon cores at 3.4 GHz, 16 GB of RAM, using a 64-bit Ubuntu 14.04 LTS operating system.

### 5.2.1 VALIDATION

In the following sections, to validate our cellular automaton model we perform the comparison with the analysis of Equation (1.1) on page 2 presented by Wattis [118] where a gel state is reached, and the expected behavior as seen in our differential-equation model represented by Equation (4.3) on page 52.

#### 5.2.1.1 ANALYSIS OF THE SMOLUCHOWSKI EQUATION

In order to validate our cellular automaton model, a comparison was performed with the analysis and hypothesis of the Smoluchowski Equation — as represented by Equation (1.1) on page 2 — presented by Wattis [118]. In the analysis, Wattis uses concentration  $c_r$  to refer the density  $\rho_n$ . One particular case of Equation (1.1) is when only the coalescence process is present. The elimination of terms of fragmentation in Smoluchowsky equation represented by Equation (1.1) on page 2 leads to a equation known as Smoluchowsky Coalescence equation:

$$\frac{d\rho_n}{dt} = \frac{1}{2} \sum_{i+j=n} [\rho_i \rho_j A_{i,j}] - \sum_{j=1}^{\infty} [\rho_n \rho_j A_{n,j}]. \quad (5.1)$$

Wattis presents different phase transitions of Equation (5.1). The theoretical analysis of Equation (5.1) presented by Wattis [118] focuses in the mass flux of the system  $J_n$  (flux of flocs with sizes less than  $k$  to flocs of larger sizes than  $k$ ):

$$J_n = \sum_{j=1}^n \left[ \sum_{i=1}^{\infty} a_{i,j} \rho_i \right] j \rho_j, \quad (5.2)$$

where the constant  $j\rho_j$  is the total mass of size  $j$  and  $\sum_{i=1}^{\infty} a_{i,j}\rho_i$  is the encounter rate of sizes  $i$  and  $j$ . A visual representation of the mass flux  $J_k$  is shown in Figure

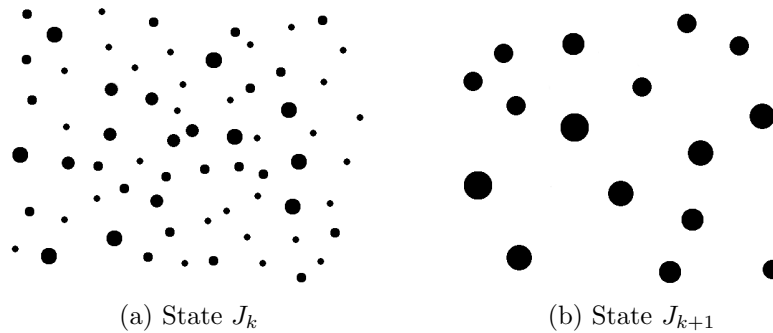


Figure 5.1: Visual representation of the mass flux of  $J_k$  to  $J_{k+1}$ . The Figure 5.1a is a state where flocs from sizes less or equal than  $k$  ( $J_k$ ) are present. When the mass flow occurs, the state  $J_{k+1}$  emerges (Figure 5.1b), where floc sizes  $k + 1$  ( $J_{k+1}$ ) are present.

5.1. If the existing flux of mass is out of the system, theoretically a *superparticle* (a floc of infinite size) is formed. The superparticle is also known as *gel*. It is assumed that the time to reach gel state in the system as the time tends to infinity according to the analysis presented by Wattis [118].

Theoretically a cellular automaton can reach a stationary state without depending on the initial state. To be consistent with the assumptions in the analysis made by Wattis [118]: to start the automaton, a total of  $n$  cells with a floc size of one (the density floc-size of one is equal to one,  $\rho_1 = 1$ ) are created, the parameter  $f$  is fixed to  $f = 1$  (pure coalescence),  $v = 0.001$  (low fragmentation rate), and the simulation stops when any cell  $c$  contains the floc of size  $n$  (gel state is reached). The total number of cells  $n$  for each dimension was set to  $n = k^d$ , where  $d$  is the dimension and  $k = \lceil \sqrt[d]{t} \rceil$ , setting  $t = 1\,000$ . A total of ten replicas are performed for dimensions from two to five; the logarithm boxplot of the number of steps needed to reach gel state are shown in Figure 5.2 for each dimension. The one-dimensional is not included due to its inability to reach the gel state within the  $2^{30}$  steps (we attempted increasing the step count but saw no progress towards a gel state for the one-dimensional case). As shown in Figure 5.2, the number of steps required for

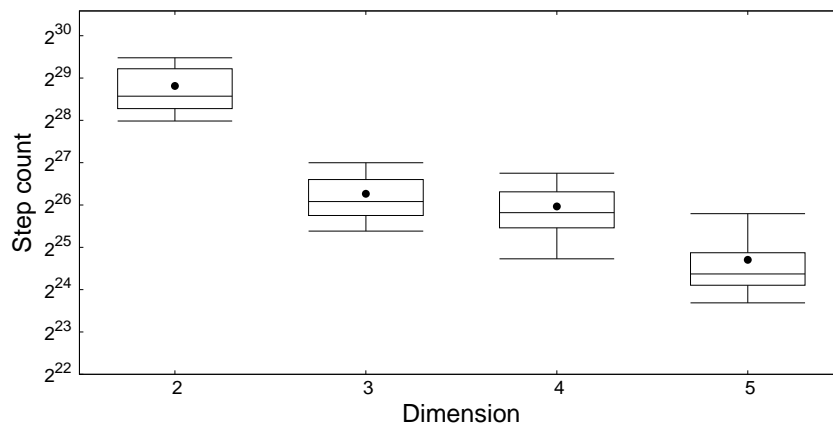


Figure 5.2: Comparison between four dimensions reaching a gel state as a function of the steps. The one-dimensional automaton is not presented because it cannot reach the gel state. For the two-dimensional automaton, all but one repetition reach the gel state.

reaching the gel state decreases as the dimension of the automaton increases.

The hypothesis for the behavior of the cellular automaton is that its structure in higher dimensions increases the number of interactions between neighbors and are better to correspond the turbulence effect of a fluid with external agitation. For example, in a one-dimensional automaton each cell  $c$  has two neighbors, but in five-dimension automaton, the number of neighbors is increased to ten. As the number of neighbors increases, the distance between cells is reduced — Figure 5.3 shows the average Manhattan distance<sup>3</sup>— in the automaton as a function of the dimension.

### 5.2.1.2 DIFFERENTIAL EQUATION MODEL

To validate the proposed cellular automaton model, we present the comparison of the analysis of our differential-equation model represented by Equation (4.3) on page 52 with the behavior of our cellular automaton. The cellular automaton model is a counterpart of the constant kernels of coalescence  $A$  and fragmentation  $F$  of our

<sup>3</sup>The sum of all the absolute values of the differences between the coordinates.

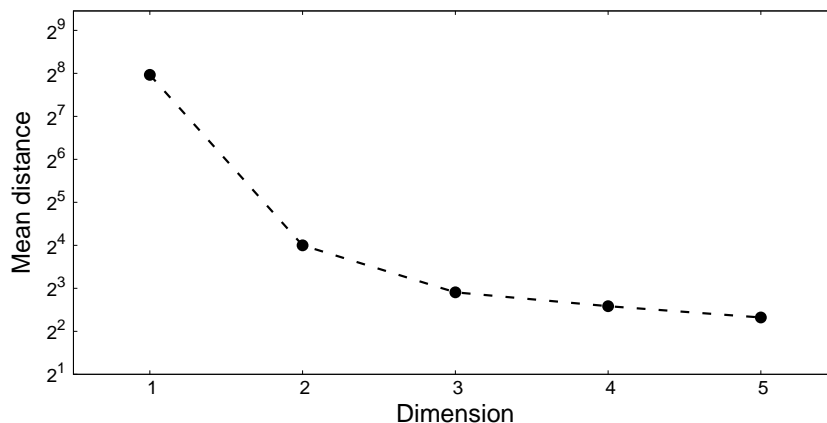


Figure 5.3: Average Manhattan distances between cells as a function of the dimension of the automaton. The total number of cells  $n$  for each dimension is set to  $n = k^d$  where  $d$  is the dimension and  $k = \lceil \sqrt[d]{t} \rceil$ .

differential-equation model.

To compare both models, we consider the following assumptions for the automaton: the average floc-size  $\bar{h}$  represents the stable floc size  $h^*$  in the model of Equation (4.3) on page 52, the *coalescence rate*  $f$  in the automaton represents the coalescence kernel  $A$ , and the *fragmentation rate*  $v$  represents the fragmentation kernel  $F$ .

The fragmentation rate  $v$  acts as the floc *instability*: if  $v \rightarrow 1$ , the flocs of sizes above the average  $\bar{h}$  are unstable and tend to fragment. The coalescence rate  $f$ , on the other hand, acts as the floc *stability*: the growth of the flocs above the average  $\bar{h}$  depends on  $f$  when  $v < 1$ . Therefore, based on the analysis of Equation (4.3) on page 52 when the coalescence rate  $A$  is constant, the limit  $\frac{F}{A} \rightarrow 0$  — low fragmentation rate and high coalescence rate — corresponds to  $f \rightarrow 1$ ,  $v \rightarrow 0$ , and the limit  $\frac{F}{A} \gg 1$  — high fragmentation rate and low coalescence rate — corresponds to  $f \rightarrow 0$  and  $v \rightarrow 1$ . According to the these analysis of both automaton and differential-equation models, we present two different cases where the automaton model capture the predicted behavior by our Smoluchowski-type model.

The first case is when the fragmentation rate is high and the coalescence rate is low (limit  $\frac{F}{A} \gg 1$ ) where the expected behavior of the first two moments of the stationary distribution (mean and variance) of Equation (4.15) on page 55 is that the mean grows linearly according to the stable size  $h^*$  and the variance grows parabolic according to the stable size  $h^*$ . Therefore, to obtain the same behavior of both the mean and the variance with our automaton model, we vary the average floc-size  $\bar{h}$  in the automaton from two to five, and set the coalescence rate  $f = 0.1$  and the fragmentation rate  $v = 0.9$ , to be consistent with the limit  $\frac{F}{A} \gg 1$ . In Figure 5.4 is clearly shown how there is a linear dependence with the average floc-size  $\bar{h}$  and in Figure 5.5 is shown that again the behavior is the same as the predicted by Equation (4.15) on page 55 in terms of the stable floc size  $h^*$ .

The second case is when the fragmentation rate is low and the coalescence rate is high (limit  $\frac{F}{A} \rightarrow 0$ ) where the expected behavior of the first two moments of the stationary distribution (mean and variance) of Equation (4.15) on page 55 is that they have large values. Therefore, to obtain the same behavior of both the mean and the variance in the limit  $\frac{F}{A} \rightarrow 0$  with our automaton model, we vary the average floc-size  $\bar{h}$  from two to five, set the coalescence rate  $f = 0.9$ , and the coalescence rate  $v = 0.1$ . In Figure 5.6 is shown the large values of mean and variance relative to  $\bar{h}$  as predicted by Equation (4.15) on page 55.

For both cases ten replicas are executed with  $10^5$  time steps of the automaton. The number of steps that take the automaton was chosen as we observed that the floc-size distribution is approximately stationary.

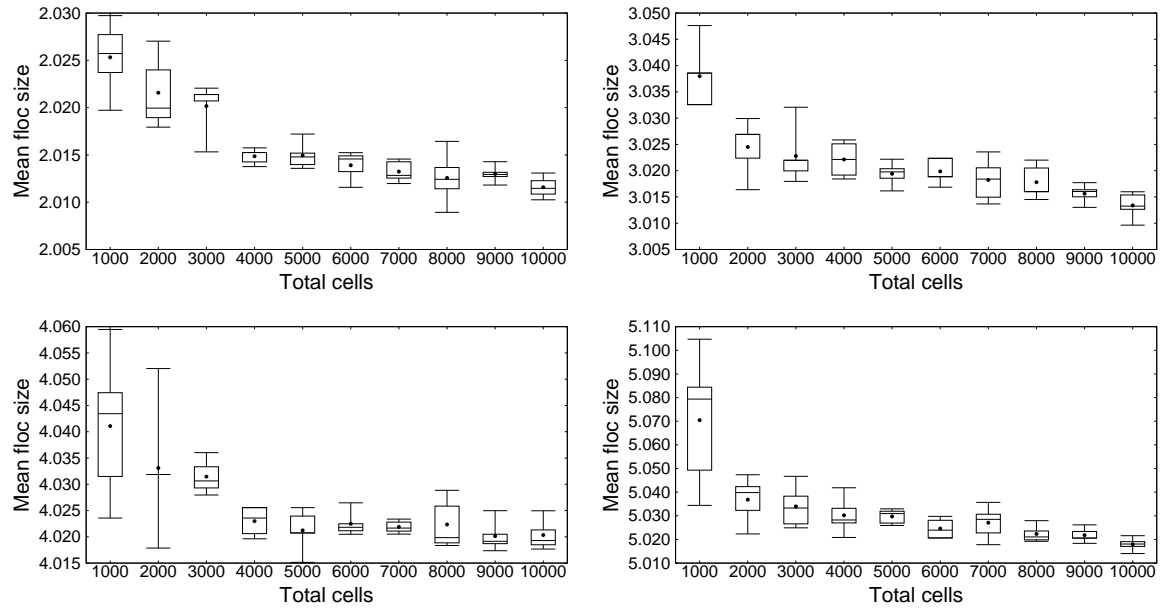


Figure 5.4: Linear growth of the floc-size distribution mean of the automaton relative to  $\bar{h}$ . The figures correspond (from left to right, top to bottom) to  $\bar{h} = \{2, 3, 4, 5\}$ . The automaton's parameters are  $f = 0.1$  and  $v = 0.9$ .

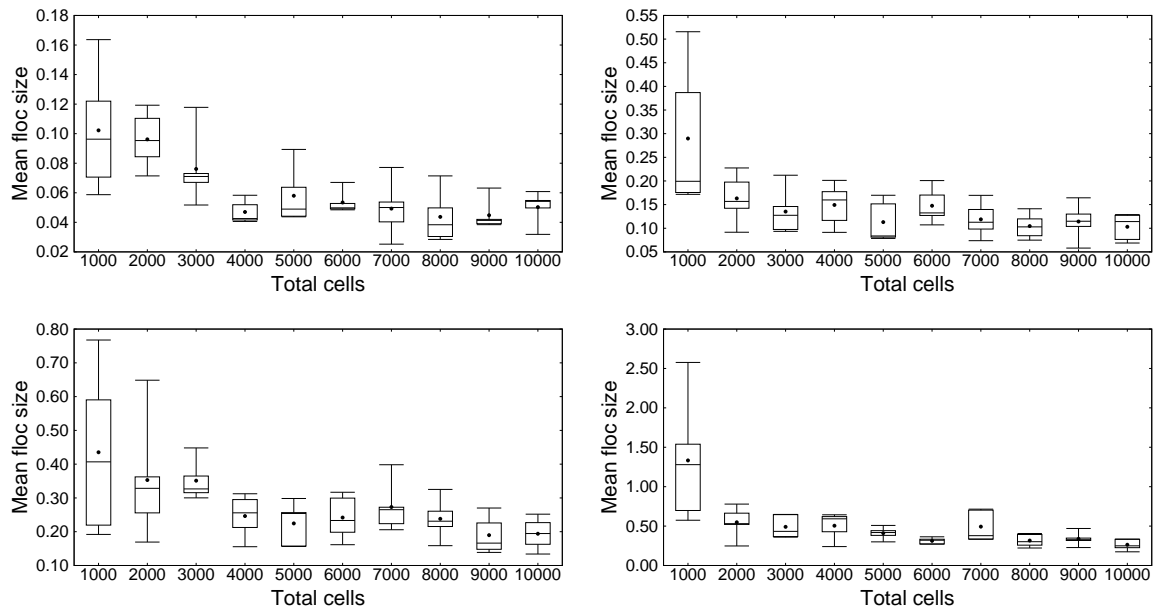


Figure 5.5: Second-order polynomial growth of the floc-size distribution variance relative to  $\bar{h}$ . The setup is the same as in Figure 5.4.

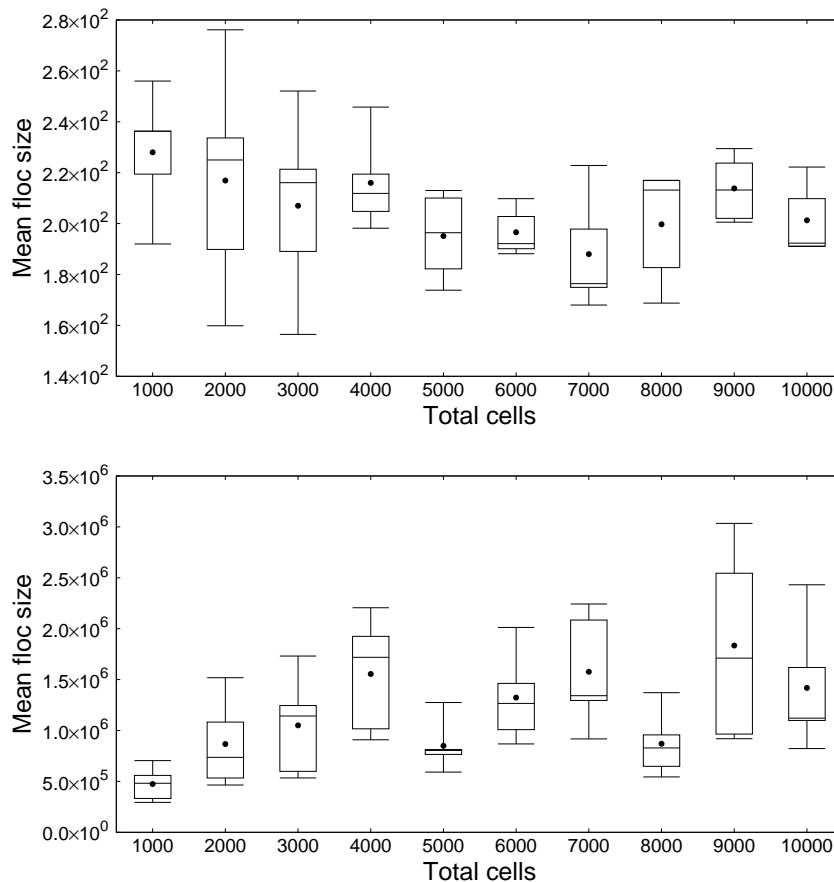


Figure 5.6: A stationary state with large mean and variance of the floc-size distribution relative to  $\bar{h} = 3$  is reported for  $f = 0.9$  and  $v = 0.1$ .

### 5.2.2 COMPARISON WITH PREVIOUS MODEL

Our implementation of the multi-dimensional extension for one-dimensional automaton can reproduce the same behavior observed in the laboratory distributions for big flocs as reported by Almaguer et al. [4]. The comparison between the models is visualized in Figure 5.7. Each laboratory floc-size distribution is chosen at the seventh minute of the experiment, each automaton-generated floc-size distribution is chosen at the  $10^6$  step, the automaton is set to one dimension, and total number of cells to 1 000. To reproduce the behavior of the previous model presented by Almaguer et al. [4], we used their assigned values for the step count, dimension, and parameters for each case; these values are shown in Table 5.1.

Table 5.1: Parameters of the simulation for the one-dimensional cellular automaton as reported by Almaguer et al. [4].

Metal	rpm	$v$	$f$
Iron	20	0.00317	0.8215
Iron	40	0.03770	0.6210
Zinc	20	0.02950	0.8440
Zinc	40	0.07390	0.6551

As the data of Almaguer et al. [4] was unavailable we extract the estimate of the coordinate of the data points of the floc-size distribution illustrated in their Figure 5 with a computational image processing coded in PYTHON using the library PIL. For both floc-size distributions it is assumed that a steady state is reached in the last step,  $10^6$ . As there is no quantitative unit that would permit scaling between the floc sizes of the automaton and laboratory data, we compare the distributions qualitatively using the shape of each distribution on a log-log scale. Figure 5.7 shows that our model has good qualitative agreement with both the previous model and the laboratory data.

### 5.2.3 PARAMETER-SPACE EXPLORATION

To characterize the relation between the coalescence rate  $f$ , fragmentation rate  $v$ , the dimension  $d$ , and the similarity between automaton-simulated and laboratory data in terms of the floc-size distribution we perform a large-scale exploration of the parameter space of the proposed multi-dimensional automaton.

Before engaging in the exploration, we perform an analysis of the laboratory experiments to quantitatively explain the evolution in time of the floc-size distribution. The analysis of the four metals — Fe 20 rpm, Fe 40 rpm, Zn 20 rpm, and Zn 40 rpm — consists in determining the evolution of the floc-size distribution for each

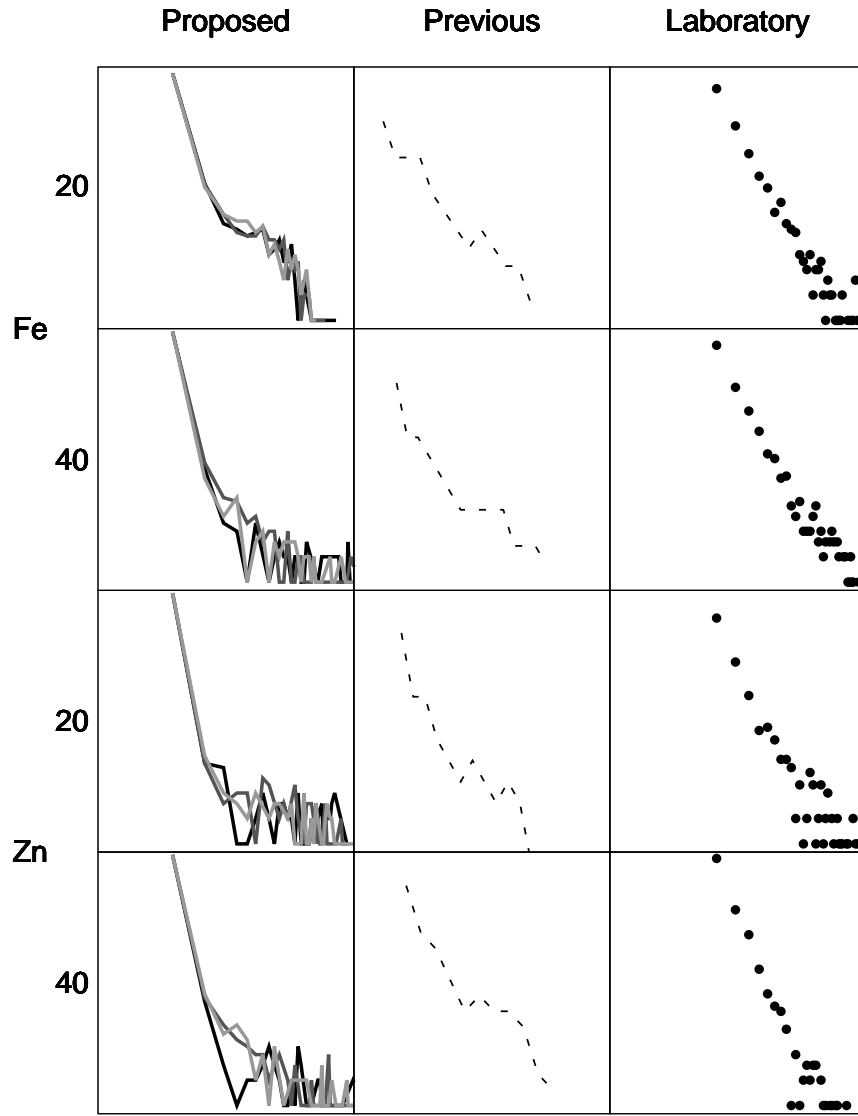


Figure 5.7: Comparison of the floc-size distribution between our one-dimensional cellular automaton (solid line), the previous one-dimensional cellular automaton from by Almaguer et al. [4] (dashed line), and the laboratory data (points). A binned histogram where the frequency is presented in the vertical axis and the floc size is presented in the horizontal axis. Both axes are in logarithmic scale. In our one-dimensional cellular automaton, a gray scale is used to differentiate the three replicas shown.

minute (1, 2, 3, 4, 5, 6, 7, and 10), specifically in terms of the proportion of flocs greater or equal to fifty micrometers. The chosen size of fifty micrometers represents the ideal scenario in which the removal of metals is efficient in wastewater treatment. For simplicity, the flocs of size above or equal to fifty micrometers are referred as

Table 5.2: Normality results for the Shapiro-Wilks test in each laboratory-experiment data using the large flocs variation. In the Test column, the laboratory experiment that do not pass the test is indicated with an  $\times$  and those that pass the test are indicated with a  $\checkmark$ .

Experiment	$p$ -value	Test
Fe20rpm	0.03012	$\times$
Fe40rpm	0.63309	$\checkmark$
Zn20rpm	0.05692	$\checkmark$
Zn40rpm	0.79581	$\checkmark$

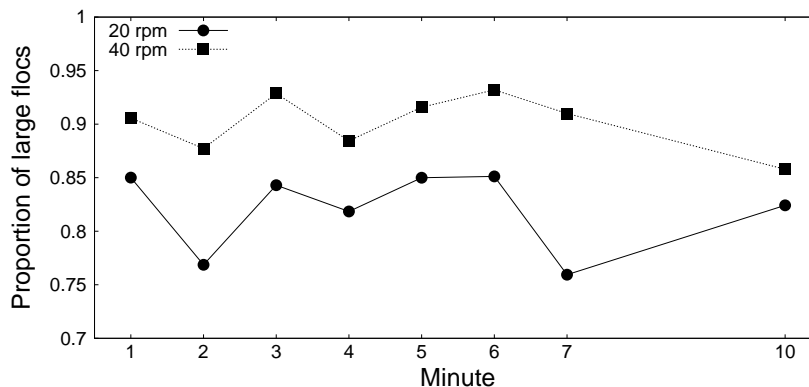
*large flocs*, and we denote the number of large flocs by  $n^{>50}$ .

The evolution of the proportion of large flocs in each laboratory floc-size distribution is presented in Figure 5.8. It is assumed that all laboratory experiments reach a *steady state* from the first minute. We want to compare the performance of the laboratory and automaton floc-size distributions in terms of the steady state evolution. A simplification in the variation of the steady state into an interval using the mean  $\bar{n}_{\text{lab}}^{>50}$  and the standard deviation  $\sigma_{\text{lab}}$  is performed. For a statistical examination of the hypothesis we performed a test for normality of the laboratory-experiment data using the Shapiro-Wilks test. The results of the test are presented in the Table 5.2 showing that three of the four laboratory experiments pass the test for normality<sup>4</sup>. We therefore assume that the proportion of large flocs during the steady state is normally distributed.

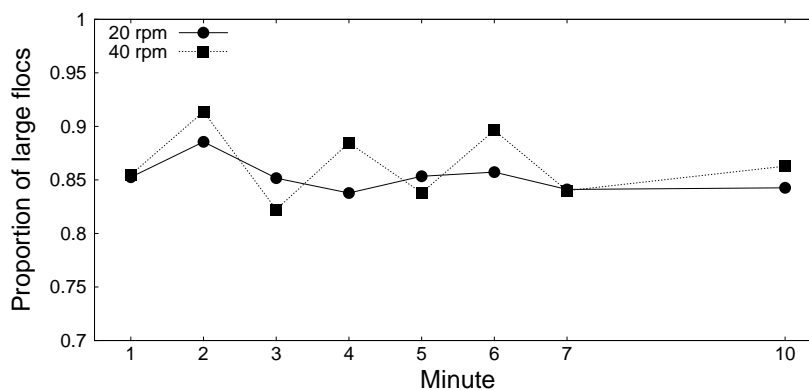
To characterize the parameter space ( $f$  and  $v$ ) and the dimension  $d$  of the proposed multi-dimensional automaton, we perform a large-scale exploration. We let both parameters  $f$  and  $v$  to take values from the set  $\{0.1, 0.2, \dots, 0.8, 0.9\}$  thus yielding a  $9 \times 9$  matrix of 81 parameter combinations, and the dimension to take values from one to five. For each combination, the total number of cells  $n$  for each

---

<sup>4</sup>If the  $p$ -value is higher than the  $\alpha = 0.05$ , the assumption of normality (null hypothesis) for the tested distribution cannot be rejected.



(a) Fe(III) experiment at speeds of 20 and 40 rpm



(b) Zn(II) experiment at speeds of 20 and 40 rpm

Figure 5.8: The four laboratory-experiment steady states in terms of the proportion of large flocs. For each of the laboratory experiment, the speed of 20 rpm is indicated as a solid line with points and the speed of 40 rpm is indicated as the dotted line with squares.

dimension was set to  $n = k^d$  where  $d$  is the dimension and  $k = \lceil \sqrt[d]{t} \rceil$  with  $t = 1000$ , and five replicas were executed. We let the automaton take  $10^5$  step count to reach the steady state for each of the simulations. To simplicity, each combination of parameters, dimension, and replica is called a *simulation*  $s$ , abbreviated as *sim*. We evaluate the effect of the parameter values in terms of the agreement of the proportion of large flocs at the steady state between the simulated and the laboratory data.

Our focus for each simulation is the same as in the laboratory experiments:

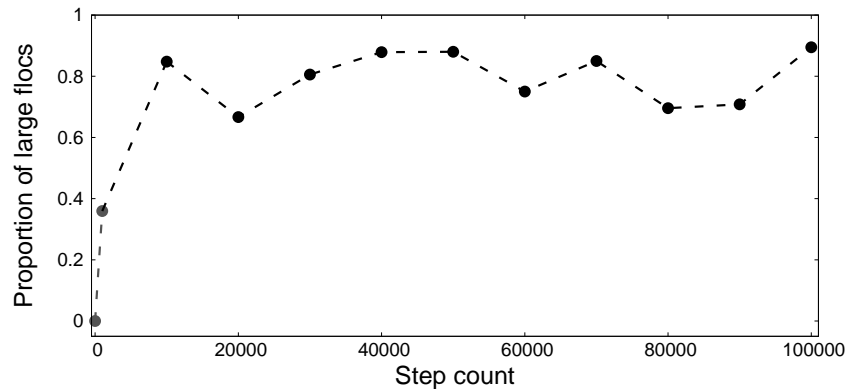


Figure 5.9: The proportion of large flocs evolution an example simulation according to the step count where a steady state and two outliers exist. The steady state is represented by the black dashed lines with points and the outliers are drawn in a gray dashed line with points.

the steady state. The number of flocs larger than the size of fifty particles  $n_{\text{sim}}^{>50}$  is obtained in all the simulations to be consistent with the laboratory experiments. Also, the flocs of size fifty particles or above are also called *large flocs* for all simulations. It is assume that a particle in the automaton is a micrometer in the laboratory experiment to easily compare the simulations with the laboratory experiments.

We perform the following procedure to obtain the section of the steady state in a simulation. First, the mean  $\bar{n}_{\text{sim}}^{>50}$  and the standard deviation  $\sigma_{\text{sim}}^{>50}$  of the large flocs of each simulation is obtained. Next, the absolute difference between the number of large flocs  $n^{>50}$  and the mean of the number of large flocs  $\bar{n}_{\text{sim}}^{>50}$  at each step of the simulation is calculated ( $\Delta n^{>50} = |n_{\text{sim}}^{>50} - \bar{n}_{\text{sim}}^{>50}|$ ). Finally, if a difference  $\Delta n^{>50}$  is greater than the standard deviation  $\sigma_{\text{sim}}^{>50}$  it is treated as an *outlier*<sup>5</sup> and removed of the simulation. A visual example of the proportion of large flocs evolution in a simulation with the presence of steady state and outliers is shown in Figure 5.9.

Again, after remove the outliers for each simulation  $s$ , the mean  $\bar{n}_{\text{sim}}^{>50}$  and the standard deviation  $\sigma_{\text{sim}}$  of the large flocs is obtained to be able to compare with the

<sup>5</sup>A value that falls outside the expected behavior of the steady state.

Table 5.3: Normality results for the Shapiro-Wilks test in a sample of the simulation data using proportion of large flocs data without outliers. In the Test column, the simulations that do not pass the test are indicated with an  $\times$  and those that pass the test are indicated with a  $\checkmark$ .

Dimension	$f$	$v$	$p$ -value	Test
1	0.7	0.1	0.6246	$\times$
1	0.8	0.2	0.1388	$\times$
1	0.9	0.2	0.0271	$\checkmark$
2	0.6	0.1	0.5517	$\times$
2	0.8	0.2	0.0205	$\times$
2	0.9	0.2	0.0125	$\checkmark$
3	0.6	0.1	0.6472	$\times$
3	0.9	0.3	0.3343	$\times$
3	0.9	0.2	0.0170	$\checkmark$
4	0.7	0.1	0.3115	$\times$
4	0.9	0.3	0.7766	$\times$
4	0.8	0.1	0.0001	$\checkmark$
5	0.6	0.8	0.0011	$\times$
5	0.7	0.6	0.3794	$\times$
5	0.7	0.1	0.0689	$\checkmark$

interval of the laboratory experiment data. Also, for each simulation  $s$  a Shapiro-Wilks test for normality was performed. The results of the test are presented in Table 5.3 showing that the majority of the simulations pass the test which is consistent with the results in laboratory data. Therefore, normality is assumed in the variation of evolution in terms of the proportion of large flocs for all simulations. We leave for future work: the exploration of every simulation where the assumption of normality is not necessary due to the hypothesis that the variation on the velocity (rpm) may deviate from normality, and the definition of an alternative interval in terms of the first and fourth quartile, or other pair of quartiles instead of the mean and standard deviation.

After the demonstration of the statistical test to use a singular interval for both laboratory and simulation data it is needed to measure some similarity between the

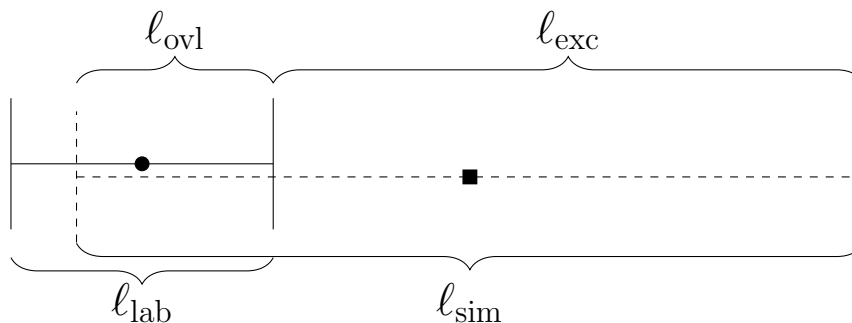
laboratory experiments and the simulation. We propose a new similarity measurement as other measurements were tested but fail to compare the distributions among their evolution: the differences between the slopes and the  $R^2$  between the laboratory data and the automaton-produced floc-size distributions, and the Sum Squared Error between the two distributions.

Before starting the definition of the proposed similarity measurement, it is obtained for each experiment and each simulation, the length of the interval by the subtraction of the upper value (mean plus the standard deviation) between the lower value (mean minus the standard deviation). Using the assumption for normality in both laboratory experiment and simulation data, the length of the interval is chosen to be two times the standard deviation ( $\ell_{\text{lab}} = 2\sigma_{\text{lab}}^{>50}$ , and  $\ell_{\text{sim}} = 2\sigma_{\text{sim}}^{>50}$ ). Therefore, the similarity measurement is defined in terms of the length of the laboratory  $\ell_{\text{lab}}$ , the length of the simulation  $\ell_{\text{sim}}$ , and the presence of an *overlap*. An overlap exists if the length of the simulation  $\ell_{\text{sim}}$  and the length of the experiment  $\ell_{\text{lab}}$  are one above the other (see Figure 5.10a). No overlap exists if the intervals are separated (see Figure 5.10b).

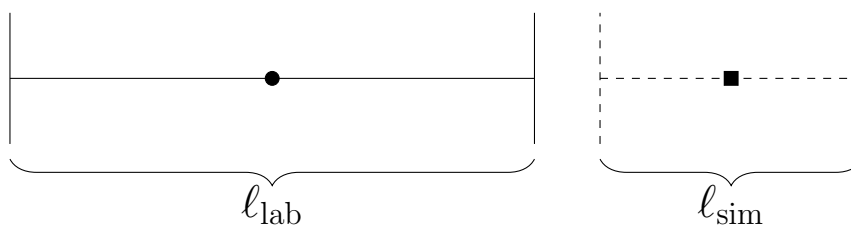
Our interest is that the overlap *cover* the whole laboratory interval and there is no *excess*. If an overlap exists, the cover  $\phi$  and the excess  $\xi$  are defined in terms of its own the length  $\ell_{\text{ovl}}$ . Besides, the cover is defined in terms of the length laboratory interval  $\ell_{\text{lab}}$ , and the excess is defined in terms of the length simulation interval  $\ell_{\text{sim}}$ . Thus, the cover  $\phi$  is obtained as a proportion between the length of the overlap  $\ell_{\text{ovl}}$  and the laboratory interval  $\ell_{\text{lab}}$ :

$$\phi = \frac{\ell_{\text{ovl}}}{\ell_{\text{lab}}}. \quad (5.3)$$

The maximum and minimum values of the cover  $\phi$  in Equation (5.3) are one and zero, respectively. The cover equal to one ( $\phi = 1$ ) indicates that the length of the overlap is the same as the length of the laboratory-experiment interval ( $\ell_{\text{ovl}} = \ell_{\text{lab}}$ ).



(a) An example with an overlap. The length interval in the simulation  $l_{\text{sim}}$  is larger than the length interval of the experiment  $l_{\text{lab}}$ .



(b) An example without an overlap. The length interval in the simulation  $l_{\text{sim}}$  is smaller than the length interval of the experiment  $l_{\text{lab}}$ .

Figure 5.10: Examples with and without an overlap between the laboratory experiment and the simulation intervals. The laboratory experiment interval is the dotted line with the mean represented as a point and the simulation interval is the solid line with a square representing the mean.

On the other hand, a cover of zero ( $\phi = 0$ ) indicates that length of the overlap is completely different that the length of the laboratory-experiment interval. In other words, as the cover is closer to one the better coverage of the overlap, and as the cover is closer to zero the worst coverage of the overlap.

The excess  $\xi$  refers to length of the simulation interval  $l_{\text{sim}}$  that is not part of the overlap (see Figure 5.10b). Therefore, the excess  $\xi$  of an overlap is obtained as a difference between the length of the simulation interval  $l_{\text{sim}}$  and the length of the overlap  $l_{\text{ovl}}$ , and normalized by the length of the simulation interval  $l_{\text{sim}}$ :

$$\xi = \frac{l_{\text{sim}} - l_{\text{ovl}}}{l_{\text{sim}}}. \quad (5.4)$$

The maximum and minimum values of the excess  $\xi$  in Equation (5.4) are one and

zero, respectively. The excess equal to one ( $\xi = 1$ ) indicates that the excess of the length of the overlap is zero as no overlap exists ( $\ell_{\text{ovl}} = 0$ ). On the other hand, an excess of zero ( $\xi = 0$ ) indicates that length of the overlap is the same as the length of the laboratory-experiment interval ( $\ell_{\text{ovl}} = \ell_{\text{lab}}$ ).

As our objective is to maximize the cover and minimize the excess of the overlap, a *similarity*  $\delta$  between the laboratory experiment and the simulation is proposed:

$$\delta = \frac{1 + \phi - \xi}{2}. \quad (5.5)$$

The maximum and minimum values of the excess  $\xi$  in Equation (5.5) are one and zero, respectively. A similarity  $\delta$  equals to one means that the laboratory interval is totally cover by the simulation interval ( $\phi = 1$ ) and there is no excess ( $\xi = 0$ ) thus, we assume that the laboratory and simulation floc-size distributions are more similar to each other. On the other hand, similarity equal to zero implies no overlap between the two intervals ( $\phi = 0$ ) and while the excess is the simulation interval as a whole ( $\xi = 1$ ).

The top five results for the comparison of each laboratory and simulation data using the similarity  $\delta$  data are shown in Table 5.4. The threshold was set at 0.59 in order to have at least five replicas above the threshold for each of the four laboratory experiments.

The results in terms of the similarity measurement are presented in Table 5.4 showing that the highest similarities have  $v$  equals to 0.1 and  $f$  equals to 0.7 or 0.8, and for the other similarities  $0.1 \leq v \leq 0.3$  and  $0.6 \leq f \leq 0.9$ . The fine-tuning of the parameters in intermediate values for  $0 < v \leq 0.2$  and  $0.6 \leq f < 1$  may lead to further improvement in the similarity between laboratory results and the simulated data but are leaved to future work as they are not considered within the

81 parameter combinations in this work.

Table 5.4 shows that the three-dimensional automaton for both the agitation speeds in the Zn(II) experiment and the one-dimensional automaton for both the agitation speeds in the Fe(III) experiment are the best at capturing the behavior of the laboratory data. Our hypothesis for this is that different coagulants are more easily to be captured by automatons of different dimensions, and in future experimentation we need to study more coagulants to demonstrate this hypothesis. Furthermore, it is shown in Table 5.4 that the variation of the agitation speed apparently produces has no systematic effect in either the best combination of  $f$  and  $v$  or in the best dimension.

The results shown in Table 5.4 for the space exploration of the parameters where greater values of coalescence rate  $f$  and lower values of fragmentation rate  $v$  matches the behavior presented in jar-test apparatus where faster agitation speed is expected to promote floc fragmentation, whereas slow agitation speed is expected to result in few interactions between flocs.

Table 5.4: Top five parameter combinations  $f$ ,  $v$ , and  $d$  of the automaton compared with each laboratory experiment using a similarity threshold greater or equal to 0.59. The maximum value of similarity  $\delta$  in each laboratory experiment is indicated in bold text.

Experiment	Dimension	$f$	$v$	$\delta$
<b>Fe20rpm</b>	<b>1</b>	<b>0.7</b>	<b>0.1</b>	<b>0.98882</b>
Fe20rpm	1	0.8	0.2	0.77515
Fe20rpm	4	0.6	0.1	0.77095
Fe20rpm	1	0.9	0.3	0.76135
Fe20rpm	2	0.8	0.2	0.74564
<b>Fe40rpm</b>	<b>1</b>	<b>0.8</b>	<b>0.1</b>	<b>0.77776</b>
Fe40rpm	3	0.7	0.1	0.69504
Fe40rpm	1	0.8	0.1	0.69275
Fe40rpm	1	0.8	0.1	0.66860
Fe40rpm	1	0.8	0.1	0.66767
<b>Zn20rpm</b>	<b>3</b>	<b>0.7</b>	<b>0.1</b>	<b>0.61183</b>
Zn20rpm	1	0.9	0.3	0.60523
Zn20rpm	2	0.8	0.2	0.59891
Zn20rpm	1	0.8	0.1	0.59667
Zn20rpm	1	0.9	0.2	0.59644
<b>Zn40rpm</b>	<b>3</b>	<b>0.7</b>	<b>0.1</b>	<b>0.73714</b>
Zn40rpm	1	0.8	0.1	0.70499
Zn40rpm	1	0.9	0.2	0.70451
Zn40rpm	4	0.7	0.1	0.70326
Zn40rpm	4	0.8	0.2	0.70009

## CHAPTER 6

# CONCLUSIONS

---

A Markovian probabilistic cellular automaton to capture the essential phenomenology of coalescence and fragmentation in the presence of external agitation was proposed and reproduced some basic features of floc-size distribution of heavy-metal wastewater removal in a jar-test apparatus. The validation of the cellular automaton was performed through the comparison with analysis and hypothesis reported by Wattis [118] and our analysis of the Smoluchowski balance equations, and the extensive numerical experiments of the parameter spaces ( $f$ ,  $v$ , and  $d$ ) was performed to identify those that best reproduce the observed floc-size distributions in laboratory data.

In this chapter the conclusions and analysis results of our proposed model are shown. First, in Section 6.1, the principal contributions in this thesis are presented. Next, in Section 6.2, it is discussed the results to our proposed models, and the general conclusion of this thesis are presented. Then, in Section 6.3, the future work to explore new methodologies and new approaches are presented.

## 6.1 CONTRIBUTIONS

A multi-dimensional extension of a Markovian probabilistic cellular automaton model that capture the expected behavior of the coalescence and fragmentation process in the presence of external agitation as shown in the laboratory-experiment of the jar-test apparatus based on the industrial wastewater treatment was proposed.

We propose a new quantitative-similarity measurement that permits the comparison with the evolution of the laboratory-observed floc-size distributions as the previous one-dimensional model presented by Almaguer et al. [4] does not include any quantitative comparison. Also, using the similarity measurement, the multi-dimensional model captures and improves the agreement of floc-size distributions for laboratory data from a heavy-metals wastewater removal experiment with high accuracy than the previous one-dimensional model presented by Almaguer et al. [4]. Therefore, the multi-dimensional model provides a computationally cheaper and intuitively appealing alternative to integro-differential coupled equations models. We propose an integro-differential coupled equations models to validate the behavior of our multi-dimensional model.

## 6.2 DISCUSSION

Our proposed multi-dimensional cellular automaton is capable of reaching the theoretical gel state as well as replicating the steady-state behavior of laboratory data. To our knowledge, our model with adjustable parameters  $f$  and  $v$  is the first general analytic model for the coalescence-fragmentation process.

We found that the best dimension according to our proposed similarity mea-

surement appears to depend on the coagulant: the laboratory experiment Fe(III) is best captured with a one-dimensional automaton while the laboratory experiment Zn(II) is best captured with a three-dimensional automaton. Also, the parameters that maximize the similarity between the laboratory data and the multi-dimensional model-generated floc-size distribution are in a limited interval for both the flocculant  $f$  and the agitation speed  $v$ . The interval for the coalescence rate  $f$  is between 0.6 and 0.9, 0.8 being the most frequent value, and for the fragmentation rate  $v$  the value never exceeds 0.3, 0.1 being the most frequent value. The future exploration of the intermediate values in  $[0.6, 0.9]$  for  $f$  is needed, with special attention to the range  $[0.7, 0.8]$ , and the exploration for  $v < 0.3$  using values  $2^i$  for  $i \leq -2$ .

### 6.3 FUTURE WORK

Further exploration is needed to improve our results for the multi-dimensional automaton model. Some characteristics to improve the multi-dimensional model are: the parameter optimization, the model performance, the effects of the neighborhood topology (including periodic boundary conditions and higher-dimensional lattices), the initial floc-size distribution, the behavior of the model with different rules, and the temporal variation of the coalescence rate  $f$  and fragmentation rate  $v$  to model experimental situations where the control parameters are not fixed but instead are adjusted during the process.

Additionally, increase the jar-test experiments using more levels for the current factors: the flocculant and the agitation speed, more factors: the concentration of the flocculant, for example, higher concentration levels reduce the coalescence's efficiency and lower levels reduce the coalescence, and more time that the experiment is leaved not only until ten minutes. Our hypothesis for the increasing in experimentation is

that more data permit statistically deduce jar-test parameters from the parameters of the best-fitting cellular automaton. In addition, it is needed to capture the behavior using an evolutionary analysis of the whole laboratory floc-size distribution not only the part of the distribution with large flocs.

Future experimentation is needed to study different behaviors of the model and the way in which it corresponds to laboratory observations of the coalescence-fragmentation process when changing the global average floc size  $\bar{h}$  to neighborhood average floc size  $\bar{h}^*$  of cell  $c$ , restructure Rule 1A and 2A (donors and receptors), or using Rule 1S and Rule 2S. Other rules of the automaton change the behavior of the model presented in this work. One of the implementation of the Rules 1A and 2A is that first, each cell  $c$  mark its states as a idle (do nothing), receptor (wiling to receive particles) or donor (share particles). Another rules are that each donor obtain how many neighbors receptors they have and share an even part of its particles to each neighbor that were receptor.

We leave for further implementation other initial configurations of the automaton as the showed in Chapter 4 and different neighborhood topologies. We also contemplate the use of a multi-agent model where the flocs move and interact instead of using cellular automaton. This approach it is only feasible with parallel computing and using GPU analysis due to the elevated of computational effort. We also plan to incorporate aspects such as the size and shape of the tank, the size, shape, movement of the paddle, and the chemical composition of the wastewater into detailed versions of our models in the future.

# BIBLIOGRAPHY

---

- [1] Ahsan, T. and Alaerts, G. (1997). Modeling separation of flocculant particles in horizontal-flow gravel bed. *Journal of Environmental Engineering*, 123(12):1254–1260.
- [2] Al-Tarazi, M., Heesink, A. B. M., and Versteeg, G. F. (2004). Precipitation of metal sulphides using gaseous hydrogen sulphide: mathematical modelling. *Chemical Engineering Science*, 59(3):567–579.
- [3] Al-Thyabat, S. and Miles, N. (2006). An improved estimation of size distribution from particle profile measurements. *Powder Technology*, 166(3):152–160.
- [4] Almaguer, F., Alcalá, M., Berrones, A., Chacón-Mondragón, O., and Soto-Regalado, E. (2013). Conceptual model of coalescence and break-up in the presence of external agitation. *Physica A: Statistical Mechanics and its Applications*, 392(8):1725–1732.
- [5] Andres, C., Réginault, P., Rochat, M., Chaillot, B., and Pourcelot, Y. (1996). Particle-size distribution of a powder: comparison of three analytical techniques. *International Journal of Pharmaceutics*, 144(2):141–146.
- [6] Aris, R. (2012). *Mathematical modeling techniques*. Courier Corporation.
- [7] Atkinson, K., Han, W., and Stewart, D. E. (2011). *Numerical solution of ordinary differential equations*, volume 108. John Wiley & Sons.

- 
- [8] Bak, P., Tang, C., and Wiesenfeld, K. (1987). Self-organized criticality: An explanation of the  $1/f$  noise. *Physical Review Letters*, 59(4):381–384.
- [9] Ban, J.-C., Chang, C.-H., Chen, T.-J., and Lin, M.-S. (2011). The complexity of permutive cellular automata. *Journal of Cellular Automata*, 6(4/5):385–397.
- [10] Banasiak, J. (2012). Global classical solutions of coagulation-fragmentation equations with unbounded coagulation rates. *Nonlinear Analysis: Real World Applications*, 13(1):91–105.
- [11] Banasiak, J. and Lamb, W. (2011). Global strict solutions to continuous coagulation-fragmentation equations with strong fragmentation. *Proceedings of the Royal Society of Edinburgh: Section A Mathematics*, 141(3):465–480.
- [12] Banasiak, J. and Lamb, W. (2012). Analytic fragmentation semigroups and continuous coagulation-fragmentation equations with unbounded rates. *Journal of Mathematical Analysis and Applications*, 391(1):312–322.
- [13] Battistoni, P., Boccadoro, R., Bolzonella, D., and Pezzoli, S. (2001). Optimization of chemical and physical pretreatments in a platform for the treatment of liquid industrial wastes. *Industrial & engineering chemistry research*, 40(21):4506–4512.
- [14] Becker, R. and Döring, W. (1935). Kinetische Behandlung der Keimbildung in übersättigten Dämpfen. *Annalen der Physik*, 416(8):719–752.
- [15] Bohin, F., Manas-Zloczower, I., and Feke, D. L. (1996). Kinetics of dispersion for sparse agglomerates in simple shear flows: application to silica agglomerates in silicone polymers. *Chemical Engineering Science*, 51(23):5193–5204.
- [16] Boisvert, J.-P., To, T. C., Berrak, A., and Jolicoeur, C. (1997). Phosphate adsorption in flocculation processes of aluminium sulphate and poly-aluminium-silicate-sulphate. *Water Research*, 31(8):1939–1946.

- [17] Bouyer, D., Line, A., Cockx, A., and Do-Quang, Z. (2001). Experimental analysis of floc size distribution and hydrodynamics in a jar-test. *Chemical Engineering Research and Design*, 79(8):1017–1024.
- [18] Boyle, J. F., Manas-Zloczower, I., and Feke, D. L. (2005). Hydrodynamic analysis of the mechanisms of agglomerate dispersion. *Powder Technology*, 153(2):127–133.
- [19] Brasil, A., Farias, T. L., and Carvalho, M. (1999). A recipe for image characterization of fractal-like aggregates. *Journal of Aerosol Science*, 30(10):1379–1389.
- [20] Brasil, A., Farias, T. L., Carvalho, M. d. G., and Koylu, U. (2001). Numerical characterization of the morphology of aggregated particles. *Journal of Aerosol Science*, 32(4):489–508.
- [21] Broizat, D. (2010). A kinetic model for coagulation–fragmentation. In *Annales de l’Institut Henri Poincaré (C) Non Linear Analysis*, volume 27, pages 809–836. Elsevier.
- [22] Bubb, J. and Lester, J. (1994). Anthropogenic heavy metal inputs to lowland river systems, a case study. The River Stour, UK. *Water, Air, and Soil Pollution*, 78(3-4):279–296.
- [23] Chaudhuri, P. P., Chowdhury, D. R., Nandi, S., and Chattopadhyay, S. (1997). *Additive Cellular Automata: Theory and Applications*, volume 1. Wiley-IEEE Computer Society Press.
- [24] Cheng, W. P., Yu, R. F., Hsieh, Y. J., Wu, S. Y., Huang, Y. W., Chen, S. M., et al. (2008). Prove the Relationship between Particle Size, Turbidity Fluctuations by Image Analysis. In *IADIS European Conf. Data Mining*, pages 170–172.
- [25] Chopard, B. and Droz, M. (1998). *Cellular Automata Modeling of Physical Systems*. Cambridge University Press, first edition.

- 
- [26] Chopard, B. and Dupuis, A. (2002). Lattice Boltzmann models: an efficient and simple approach to complex flow problems. *Computer Physics Communications*, 147(1-2):509–515.
- [27] Chopard, B. and Luthi, P. O. (1999). Lattice Boltzmann computations and applications to physics. *Theoretical Computer Science*, 217(1):115–130.
- [28] Chopard, B. and Masselot, A. (1999). Cellular automata and lattice Boltzmann methods: a new approach to computational fluid dynamics and particle transport. *Future Generation Computer Systems*, 16(2):249–257.
- [29] Chopard, B., Masselot, A., and Dupuis, A. (2000). A lattice gas model for erosion and particles transport in a fluid. *Computer Physics Communications*, 129(1-3):167–176.
- [30] Cieplak, M. (1995). Rupture and coalescence in two-dimensional cellular automata fluids. *Physical Review E*, 51(5):4353–4361.
- [31] Clark, J., Kiwi, M., Torres, F., Rogan, J., and Valdivia, J. A. (2015). Generalization of the ehrenfest urn model to a complex network. *Physical Review E*, 92(1):012103.
- [32] Collier, A. P. and Hounslow, M. J. (1999). Growth and aggregation rates for calcite and calcium oxalate monohydrate. *American Institute of Chemical Engineers Journal*, 45(11):2298–2305.
- [33] D’ambrosio, D., Di Gregorio, S., Gabriele, S., and Gaudio, R. (2001). A cellular automata model for soil erosion by water. *Physics and Chemistry of the Earth, Part B: Hydrology, Oceans and Atmosphere*, 26(1):33–39.
- [34] De la Peña, M. E., Ducci, J., and Zamora Plascencia, V. (2013). Tratamiento de aguas residuales en México. Technical report, Inter-American Development Bank.

- 
- [35] Di Gregorio, S. and Serra, R. (1999). An empirical method for modelling and simulating some complex macroscopic phenomena by cellular automata. *Future generation computer systems*, 16(2):259–271.
- [36] Di Gregorio, S., Serra, R., and Villani, M. (1999). Applying cellular automata to complex environmental problems: The simulation of the bioremediation of contaminated soils. *Theoretical Computer Science*, 217(1):131–156.
- [37] Di Lena, P. and Margara, L. (2008). Computational complexity of dynamical systems: the case of cellular automata. *Information and Computation*, 206(9-10):1104–1116.
- [38] Dym, C. (2004). *Principles of mathematical modeling*. Academic press.
- [39] Dzwinel, W., Alda, W., and Yuen, D. (1999). Cross-scale numerical simulations using discrete particle models. *Molecular Simulation*, 22(6):397–418.
- [40] Elminyaw, I., Gangopadhyay, S., and Sorensen, C. (1991). Numerical solutions to the Smoluchowski aggregation-fragmentation equation. *Journal of Colloid and Interface Science*, 144(2):315–323.
- [41] Ernst, M., van Velzen, G., and Binder, P. (1989). Breakdown of the Boltzmann equation in cellular-automata lattice gases. *Physical Review A*, 39(8):4327–4329.
- [42] Family, F., Meakin, P., and Deutch, J. (1986). Kinetics of coagulation with fragmentation: scaling behavior and fluctuations. *Physical Review Letters*, 57(6):727–730.
- [43] Faybishenko, B., Benson, S. M., Gale, J. E., and Molz, F. (2015). A complex systems approach to describing flow and transport in fractured-porous media. *Fluid Dynamics in Complex Fractured-Porous Systems*, 7(5):5–17.

- 
- [44] Fishman, G. (2013). *Discrete-event simulation: modeling, programming, and analysis*. Springer Science & Business Media.
- [45] Flajolet, P., Dumas, P., and Puyhaubert, V. (2006). Some exactly solvable models of urn process theory. In *Fourth Colloquium on Mathematics and Computer Science Algorithms, Trees, Combinatorics and Probabilities*, pages 59–118. Discrete Mathematics and Theoretical Computer Science.
- [46] Flesch, J. C., Spicer, P. T., and Pratsinis, S. E. (1999). Laminar and turbulent shear-induced flocculation of fractal aggregates. *American Institute of Chemical Engineers Journal*, 45(5):1114–1124.
- [47] Franceschi, M., Girou, A., Carro-Diaz, A., Maurette, M., and Puech-Costes, E. (2002). Optimisation of the coagulation-flocculation process of raw water by optimal design method. *Water Research*, 36(14):3561–3572.
- [48] Gmachowski, L. (2002). Calculation of the fractal dimension of aggregates. *Colloids and Surfaces A: Physicochemical and Engineering Aspects*, 211(2):197–203.
- [49] Gorelick, M. and Ozsvald, I. (2014). *High Performance Python: Practical Performant Programming for Humans*. Micha Gorelick, Ian Ozsvald.
- [50] Grinstein, G., Jayaprakash, C., and He, Y. (1985). Statistical mechanics of probabilistic cellular automata. *Physical Review Letters*, 55(23):2527–2530.
- [51] Gupta, A. and Kumar, R. (2008). Lattice Boltzmann simulation to study multiple bubble dynamics. *International Journal of Heat and Mass Transfer*, 51(21):5192–5203.
- [52] Gutowitz, H. (1991). *Cellular automata: theory and experiment*. MIT press, first edition.

- [53] Haslam, I. W., Crouch, R. S., and Seaid, M. (2008). Coupled finite element-lattice Boltzmann analysis. *Computer Methods in Applied Mechanics and Engineering*, 197(51):4505–4511.
- [54] Higbie, R. (1935). The rate of absorption of a pure gas into a still liquid during short periods of exposure. *Translational American Institute of Chemical Engineers*, 31:365–389.
- [55] Higuera, F. and Jimenez, J. (1989). Boltzmann approach to lattice gas simulations. *Europhysics Letters*, 9(7):663–668.
- [56] Hill, P. J. and Ng, K. M. (2002). Particle size distribution by design. *Chemical Engineering Science*, 57(12):2125–2138.
- [57] Himmelblau, D. M. and Bischoff, K. B. (1968). *Process analysis and simulation: deterministic systems*. Wiley.
- [58] Jiang, J. and Graham, N. (1998). Observations of the comparative hydrolysis/precipitation behaviour of polyferric sulphate and ferric sulphate. *Water Research*, 32(3):930–935.
- [59] Kang, L.-S. and Cleasby, J. L. (1995). Temperature effects on flocculation kinetics using Fe (III) coagulant. *Journal of Environmental Engineering*, 121(12):893–901.
- [60] Kari, J. (2005). Theory of cellular automata: A survey. *Theoretical Computer Science*, 334(1-3):3–33.
- [61] Kier, L. B., Seybold, P. G., and Cheng, C.-K. (2005). *Modeling chemical systems using cellular automata*, volume 1. Springer Science & Business Media.
- [62] Kinzel, W. (1985). Phase transitions of cellular automata. *Zeitschrift für Physik B Condensed Matter*, 58(3):229–244.

- [63] Kiparissides, C., Alexopoulos, A., Roussos, A., Dompazis, G., and Kotoulas, C. (2004). Population balance modeling of particulate polymerization processes. *Industrial & Engineering Chemistry Research*, 43(23):7290–7302.
- [64] Ko, Y.-D. and Shang, H. (2011). A neural network-based soft sensor for particle size distribution using image analysis. *Powder Technology*, 212(2):359–366.
- [65] Korner, C., Thies, M., and Singer, R. F. (2002). Modeling of metal foaming with lattice Boltzmann automata. *Advanced Engineering Materials*, 4(10):765–769.
- [66] Kumar, J., Peglow, M., Warnecke, G., and Heinrich, S. (2008a). The cell average technique for solving multi-dimensional aggregation population balance equations. *Computers & Chemical Engineering*, 32(8):1810–1830.
- [67] Kumar, J., Peglow, M., Warnecke, G., and Heinrich, S. (2008b). An efficient numerical technique for solving population balance equation involving aggregation, breakage, growth, and nucleation. *Powder Technology*, 182(1):81–104.
- [68] Kumar, J., Peglow, M., Warnecke, G., Heinrich, S., and Mörl, L. (2006). Improved accuracy and convergence of discretized population balance for aggregation: The cell average technique. *Chemical Engineering Science*, 61(10):3327–3342.
- [69] Kumar, J., Warnecke, G., Peglow, M., and Heinrich, S. (2009). Comparison of numerical methods for solving population balance equations incorporating aggregation and breakage. *Powder Technology*, 189(2):218–229.
- [70] Kumar, R. G., Strom, K. B., and Keyvani, A. (2010). Floc properties and settling velocity of San Jacinto estuary mud under variable shear and salinity conditions. *Continental Shelf Research*, 30(20):2067–2081.

- [71] Kumar, S. and Ramkrishna, D. (1996). On the solution of population balance equations by discretization-i. A fixed pivot technique. *Chemical Engineering Science*, 51(8):1311–1332.
- [72] Kumar, S. and Ramkrishna, D. (1997). On the solution of population balance equations by discretization-III. Nucleation, growth and aggregation of particles. *Chemical Engineering Science*, 52(24):4659–4679.
- [73] Lement B. Kier, Paul G. Seybold, C.-K. C. (2005). *Modeling Chemical Systems using Cellular Automata*, volume 1. Springer Netherlands.
- [74] Lent, C. S., Tougaw, P. D., Porod, W., and Bernstein, G. H. (1993). Quantum cellular automata. *Nanotechnology*, 4(1):49–57.
- [75] Lewis, A. E. (2010). Review of metal sulphide precipitation. *Hydrometallurgy*, 104(2):222–234.
- [76] Li, X.-y., Zhang, J.-j., and Lee, J. H. (2004). Modelling particle size distribution dynamics in marine waters. *Water Research*, 38(5):1305–1317.
- [77] Lomnitz-Adler, J. (1993). Automaton models of seismic fracture: constraints imposed by the magnitude-frequency relation. *Journal of Geophysical Research: Solid Earth*, 98(B10):17745–17756.
- [78] Mahoney, A. W. and Ramkrishna, D. (2002). Efficient solution of population balance equations with discontinuities by finite elements. *Chemical Engineering Science*, 57(7):1107–1119.
- [79] Manneville, P., Boccara, N., Vichniac, G. Y., and Bidaux, R. (2012). *Cellular Automata and Modeling of Complex Physical Systems: Proceedings of the Winter School, Les Houches, France, February 21–28, 1989*, volume 46. Springer Science & Business Media.

- [80] Manning, A. and Dyer, K. (1999). A laboratory examination of flocculation characteristics with regard to turbulent shearing. *Marine Geology*, 160(1):147–170.
- [81] Manning, A. and Dyer, K. (2007). Mass settling flux of fine sediments in northern european estuaries: measurements and predictions. *Marine Geology*, 245(1):107–122.
- [82] Marković, D. and Gros, C. (2014). Power laws and self-organized criticality in theory and nature. *Physics Reports*, 536(2):41–74.
- [83] Masters, G. M. and Ela, W. (2008). *Introduction to environmental engineering and science*, volume 3. Prentice Hall Englewood Cliffs, NJ.
- [84] Mazoyer, J. and Terrier, V. (1999). Signals in one-dimensional cellular automata. *Theoretical Computer Science*, 217(1):53–80.
- [85] Meyer, D. A. (1996). From quantum cellular automata to quantum lattice gases. *Journal of Statistical Physics*, 85(5-6):551–574.
- [86] Mokhtari, T., Chakrabarti, A., Sorensen, C. M., Cheng, C.-y., and Vigil, D. (2008). The effect of shear on colloidal aggregation and gelation studied using small-angle light scattering. *Journal of Colloid and Interface Science*, 327(1):216–223.
- [87] Nowak, K. (2011). Grain size dependence of creep lifetime modeled by means of cellular automata. *Acta Mechanica et Automatica*, 5(4):81–85.
- [88] Packard, N. H. and Wolfram, S. (1985). Two-dimensional cellular automata. *Journal of Statistical Physics*, 38(5):901–946.
- [89] Perumal, D. A. and Dass, A. K. (2015). A review on the development of lattice Boltzmann computation of macro fluid flows and heat transfer. *Alexandria Engineering Journal*, 54(4):955–971.

- 
- [90] Qamar, S. and Warnecke, G. (2007). Numerical solution of population balance equations for nucleation, growth and aggregation processes. *Computers & Chemical Engineering*, 31(12):1576–1589.
- [91] Ramkrishna, D. (2000). *Population balances: Theory and applications to particulate systems in engineering*. Academic Press.
- [92] Ramkrishna, D. and Mahoney, A. W. (2002). Population balance modeling. Promise for the future. *Chemical Engineering Science*, 57(4):595–606.
- [93] Ramphal, S. and Sibiya, M. (2014). Optimization of coagulation-flocculation parameters using a photometric dispersion analyser. *Drinking Water Engineering and Science*, 7(2):73–82.
- [94] Reed, W. H. and Hill, T. (1973). Triangular mesh methods for the neutron transport equation. Technical report, Los Alamos Scientific Lab., N. Mex.(USA).
- [95] Reynolds, T. (1977). *Unit operations and processes in environmental engineering*. The PWS-Kent series in civil engineering. Brooks/Cole, Engineering Division, Wadsworth, CA, USA.
- [96] Rollié, S., Briesen, H., and Sundmacher, K. (2009). Discrete bivariate population balance modelling of heteroaggregation processes. *Journal of Colloid and Interface Science*, 336(2):551–564.
- [97] Ross, S. M. (2014). *Introduction to probability models*. Academic press.
- [98] Rossini, M., Garrido, J. G., and Galluzzo, M. (1999). Optimization of the coagulation-flocculation treatment: influence of rapid mix parameters. *Water Research*, 33(8):1817–1826.
- [99] Satterfield, Z. (2005). Jar testing. *Tech Brief*, 5(1):1–4.

- [100] Seybold, P. G., Kier, L. B., and Cheng, C.-K. (1997). Simulation of first-order chemical kinetics using cellular automata. *Journal of Chemical Information and Computer Sciences*, 37(2):386–391.
- [101] Silva, M., Mater, L., Souza-Sierra, M., Corrêa, A., Sperb, R., and Radetski, C. (2007). Small hazardous waste generators in developing countries: use of stabilization/solidification process as an economic tool for metal wastewater treatment and appropriate sludge disposal. *Journal of Hazardous Materials*, 147(3):986–990.
- [102] Singh, V., Banerjee, V., and Sharma, M. (2009). Dynamics of magnetic nanoparticle suspensions. *Journal of Physics D: Applied Physics*, 42(24):245006.
- [103] Sipper, M. and Tomassini, M. (1999). Computation in artificially evolved, non-uniform cellular automata. *Theoretical Computer Science*, 217(1):81–98.
- [104] Smoluchowski, M. v. (1918). Versuch einer mathematischen Theorie der Koagulationskinetik kolloider Lösungen. *Zeitschrift für Physikalische Chemie*, 92(1):129–168.
- [105] Somers, J. (1993). Direct simulation of fluid flow with cellular automata and the lattice-Boltzmann equation. *Applied Scientific Research*, 51(1):127–133.
- [106] Soos, M., Sefcik, J., and Morbidelli, M. (2006). Investigation of aggregation, breakage and restructuring kinetics of colloidal dispersions in turbulent flows by population balance modeling and static light scattering. *Chemical Engineering Science*, 61(8):2349–2363.
- [107] Soos, M., Wang, L., Fox, R., Sefcik, J., and Morbidelli, M. (2007). Population balance modeling of aggregation and breakage in turbulent Taylor-Couette flow. *Journal of Colloid and Interface Science*, 307(2):433–446.
- [108] Spiegel, M. R., Schiller, J. J., Srinivasan, R. A., and LeVan, M. (2009). *Probability and statistics*. Mcgraw-hill New York, USA.

- 
- [109] Subbiah, R., Sastry, C., and Agamuthu, P. (2000). Removal of zinc from rubber thread manufacturing industry wastewater using chemical precipitant/flocculant. *Environmental Progress*, 19(4):299–304.
- [110] Tansel, B. and Sevimoglu, O. (2006). Coalescence and size distribution characteristics of oil droplets attached on flocs after coagulation. *Water, Air, & Soil Pollution*, 169(1):293–302.
- [111] Tome, T. and de Felicio, J. R. D. (1996). Probabilistic automaton describing a biological immunessystem. *The American Physical Society*, 53(4):3976–3981.
- [112] Tseng, C.-H., Kao, Y.-M., and Cheng, C.-H. (2017). Ehrenfest urn model with interaction. *Physical Review E*, 96(3):032125.
- [113] Verkoeijen, D., Pouw, G. A., Meesters, G. M., and Scarlett, B. (2002). Population balances for particulate processes - a volume approach. *Chemical Engineering Science*, 57(12):2287–2303.
- [114] Verney, R., Lafite, R., Brun-Cottan, J. C., and Le Hir, P. (2011). Behaviour of a floc population during a tidal cycle: laboratory experiments and numerical modelling. *Continental Shelf Research*, 31(10):S64–S83.
- [115] Vigil, R. D. (2009). On equilibrium solutions of aggregation-fragmentation problems. *Journal of Colloid and Interface Science*, 336(2):642–647.
- [116] Waldner, M. H., Sefcik, J., Soos, M., and Morbidelli, M. (2005). Initial growth kinetics and structure of colloidal aggregates in a turbulent coagulator. *Powder Technology*, 156(2):226–234.
- [117] Walpole, R. E., Myers, R. H., Myers, S. L., and Ye, K. (1993). *Probability and statistics for engineers and scientists*, volume 5. Macmillan New York.

- [118] Wattis, J. (2006). An introduction to mathematical models of coagulation-fragmentation processes: A discrete deterministic mean-field approach. *Physica D: Nonlinear Phenomena*, 222(1–2):1–20.
- [119] Wilking, J., Graves, S., Chang, C., Meleson, K., Lin, M., and Mason, T. (2006). Dense cluster formation during aggregation and gelation of attractive slippery nanoemulsion droplets. *Physical Review Letters*, 96(1):015501–1–015501–4.
- [120] Winterwerp, J. (2002). On the flocculation and settling velocity of estuarine mud. *Continental Shelf Research*, 22(9):1339–1360.
- [121] Wolfram, S. (1983). Statistical mechanics of cellular automata. *Modern Physics*, 55(3):601–644.
- [122] Wolfram, S. (2002). *A New Kind of Science*. Wolfram Media.
- [123] Xu, F., Wang, D.-P., and Riemer, N. (2008). Modeling flocculation processes of fine-grained particles using a size-resolved method: comparison with published laboratory experiments. *Continental Shelf Research*, 28(19):2668–2677.
- [124] Xu, F., Wang, D.-P., and Riemer, N. (2010). An idealized model study of flocculation on sediment trapping in an estuarine turbidity maximum. *Continental Shelf Research*, 30(12):1314–1323.
- [125] Yaku, T. (1973). The constructibility of a configuration in a cellular automaton. *Journal of Computer and System Sciences*, 7(5):481–496.
- [126] Yan, F., Feng, X.-T., Pan, P.-Z., and Li, S.-J. (2014). A continuous-discontinuous cellular automaton method for cracks growth and coalescence in brittle material. *Acta Mechanica Sinica*, 30(1):73–83.
- [127] Zahnw, J. C., Maerz, J., and Feudel, U. (2011). Particle-based modeling

---

of aggregation and fragmentation processes: Fractal-like aggregates. *Physica D: Nonlinear Phenomena*, 240(9):882–893.

# RESUMEN AUTOBIOGRÁFICO

---

M. C. Luis Alejandro Benavides Vázquez

Candidato para obtener el grado de  
Doctorado en Ingeniería  
con Especialidad en Ingeniería de Sistemas

Universidad Autónoma de Nuevo León  
Facultad de Ingeniería Mecánica y Eléctrica

Tesis:

OPTIMIZACIÓN E INFERENCIA EN PROCESOS FÍSICO-QUÍMICOS  
REPRESENTADOS MEDIANTE AUTÓMATAS CELULARES

Nací el 28 de septiembre de 1989 en la ciudad de Monterrey, México. En el año 2007 ingresé a la Facultad de Ciencias Químicas de la Universidad Autónoma de Nuevo León en donde realicé mis estudios de Ingeniería Química terminando en diciembre del 2011. En el 2013 obtuve el grado Maestría en Ciencias en Ingeniería de Sistemas en el Posgrado de Ingeniería de Sistemas de la Facultad de Ingeniería Mecánica y Eléctrica de la Universidad Autónoma de Nuevo León, mediante la tesis titulada: “Detección de fugas en los procesos de una refinería”.